(NASA-CR-145965) THE EFFECTS OF RANDOM PATH FLUCTUATIONS ON THE ACCURACY OF LASER RANGING SYSTEMS (Illinois Univ.) 56 p HC $4.50

CSCL 20E

N76-14448

Unclas

G3/36 06800

THE EFFECTS OF RANDOM PATH FLUCTUATIONS ON THE ACCURACY OF LASER RANGING SYSTEMS

By

C. S. Gardner

N. Narayana Rao

RRL PUBLICATION NO. 469

DECEMBER 1975

Supported By

Contract No. NASA NSG 5049

NATIONAL AERONAUTICS & SPACE ADMINISTRATION
Goddard Space Flight Center
Greenbelt, Maryland 20771

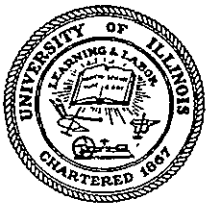

RADIO RESEARCH LABORATORY
DEPARTMENT OF ELECTRICAL ENGINEERING
COLLEGE OF ENGINEERING
UNIVERSITY OF ILLINOIS
URBANA, ILLINOIS 61801

UILU-ENG-75-2552

THE EFFECTS OF RANDOM PATH FLUCTUATIONS ON THE ACCURACY OF LASER RANGING SYSTEMS

By

C. S. Gardner

N. Narayana Rao

RRL PUBLICATION NO. 469

DECEMBER 1975

Supported By

Contract No. NASA NSG 5049

NATIONAL AERONAUTICS & SPACE ADMINISTRATION
Goddard Space Flight Center
Greenbelt, Maryland 20771

RADIO RESEARCH LABORATORY
DEPARTMENT OF ELECTRICAL ENGINEERING
COLLEGE OF ENGINEERING
UNIVERSITY OF ILLINOIS
URBANA, ILLINOIS 61801

TABLE OF CONTENTS

LIST OF ILLUSTRATIONS

1. INTRODUCTION

Laser ranging systems have developed to the point where it may now be possible to measure the distance from an orbiting satellite to a point on the earth with uncertainties on the order of only a few centimeters. The precision of satellite ranging systems will be limited in part by atmospheric refraction and scattering. In this paper the effects of atmospheric turbulence on the accuracy of single color and multicolor ranging systems is discussed. The statistical characteristics of the random path length fluctuations induced by turbulence are examined. Correlation and structure functions are derived using several proposed models for the variation of C_n^2 with altitude. For single color systems it is shown that the random path length fluctuations can limit the accuracy of a range measurement to a few centimeters. Two color systems can partially correct for the random path fluctuations so that in most cases their accuracy is limited to a few millimeters. However, at low elevation angles and over long horizontal paths two color systems can also have errors approaching a few centimeters.

2. RANDOM PATH LENGTH FLUCTUATIONS

2.1 Theoretical Background

Refractive index fluctuations caused by atmospheric turbulence will induce random variations in the optical path length. The magnitude of these path length variations can be estimated from the theoretical analyses of optical phase fluctuations published by Tatarski [1] and other workers. The instantaneous path diviation ΔL can be predicted using geometric optics

$$\Delta L = \int_C d\underline{r}\, n_1(\underline{r}). \tag{1}$$

n_1 is the fluctuating part of the refractive index about the mean value and C is the ray path. If random variations in the ray path due to n_1 are neglected,* C will be determined by the average refractivity. The average path deviation is zero because the average value of n_1 is zero

$$\langle \Delta L \rangle = \int_C d\underline{r}\, \langle n_1(\underline{r}) \rangle = 0. \tag{2}$$

The covariance between the deviations along two different paths can be written in terms of the refractive index covariance

$$B_{\Delta L} = \int_{C_1} d\underline{r}_1 \int_{C_2} d\underline{r}_2\, \langle n_1(\underline{r}_1) n_1(\underline{r}_2) \rangle. \tag{3}$$

We will assume that the refractive index is isotropic and its covariance is given as the product of a function depending on the magnitude of the difference coordinate and another function depending on the average coordinate

$$\langle n_1(\underline{r}_1) n_1(\underline{r}_2) \rangle = B_n^{\nu}\left(\frac{\underline{r}_1 + \underline{r}_2}{2}\right) B_n^{o}(|\underline{r}_1 - \underline{r}_2|). \tag{4}$$

B_n^o measures the correlation between the fluctuations at points $\underline{r}_1$ and $\underline{r}_2$ while B_n^{ν} measures the strength (variance) of the fluctuations. When the paths are identical ($C_1 = C_2$), (3) gives the mean-square deviation.

* It can be shown that variations in C due to n_1 will increase the optical path length by at most a few nm.

Two different path geometries will be considered in this paper (Figure 1). The angular path separation would be encountered with a stationary ranging site and a moving target such as a satellite. The parallel path separation would be encountered when the ranging site and target are moving in the same direction at identical speeds or when both site and target are stationary and there is a uniform wind blowing transverse to the path. To simplify the problem we will assume that the propagation paths are straight lines. Refractivity gradients in the atmosphere will cause the actual propagation paths to deviate from a straight line by as much as a few meters, particularly along the satellite path at low elevation angles. However, the deviation will only be significant at the higher altitudes where B_n^ν is small. Hence, the error will also be small. For horizontal paths, the curvature is negligible.

The parallel path covariance is calculated by substituting (4) in (3) and noting the geometry in Figure 1

$$B_{\Delta L}(d) = 4 \int_o^L dr_1 \int_o^L dr_2 \, B_n^\nu\left(\frac{r_1 + r_2}{2}\right) B_n^o \left[((r_1 - r_2)^2 + d^2)^{\frac{1}{2}}\right]. \tag{5}$$

The constant 4 appears in equation (5) because we are considering a complete "roundtrip" between the ranging site and target. Equation (5) can be rewritten in a more convenient form by making the change of variables $(r_1 + r_2)/2 = \xi$ and $(r_1 - r_2) = \rho$

$$B_{\Delta L}(d) = 8 \int_o^L d\rho \int_{\rho/2}^{L-\rho/2} d\xi \, B_n^\nu(\xi) \, B_n^o \left[(\rho^2 + d^2)^{\frac{1}{2}}\right]. \tag{6}$$

The correlation length of the refractive index fluctuations is on the order of the outer scale of turbulence, L_o. If the path length L is much larger than L_o, the upper limit on the ρ integration can be set equal to infinity and the ξ integration can be extended from 0 to L

$$B_{\Delta L}(d) = 8 \int_o^L d\xi \, B_n^\nu(\xi) \int_o^\infty d\rho \, B_n^o \left[(\rho^2 + d^2)^{\frac{1}{2}}\right]. \tag{7}$$

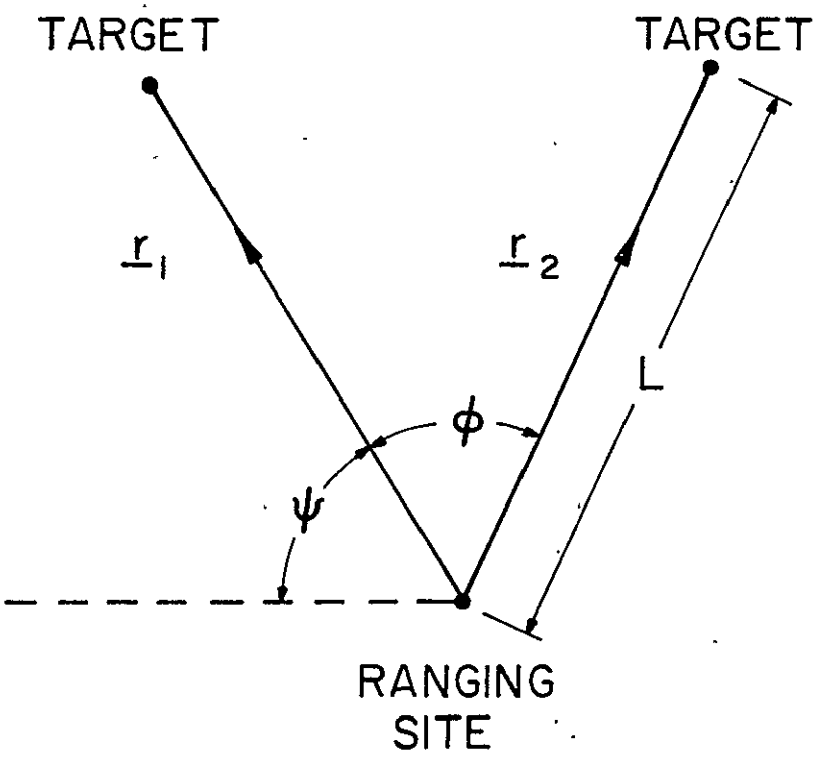

ANGULAR PATH GEOMETRY

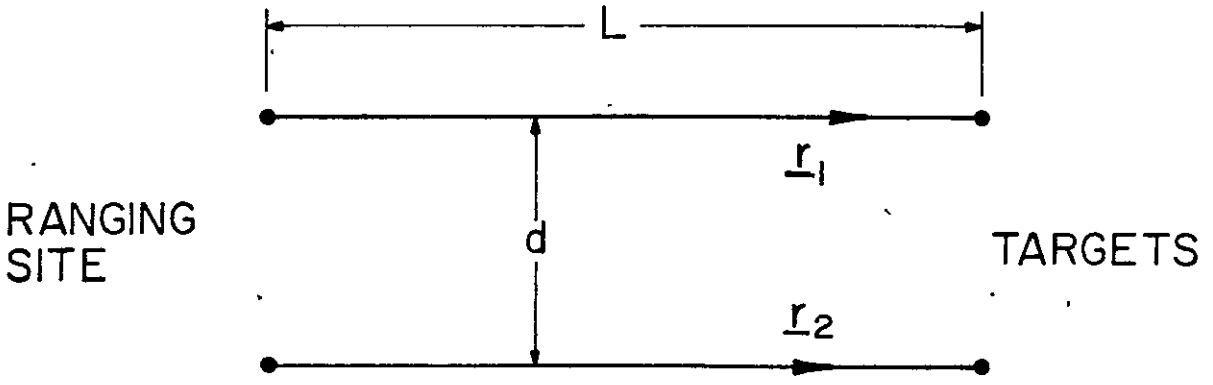

PARALLEL PATH GEOMETRY

Figure 1. Geometry of the laser ranging site and targets.

The error introduced by this approximation is on the order of $\frac{L_o}{L}$.

B_n^o can be conveniently described in terms of its spatial spectrum

$$B_n^o(r) = 4\pi \int_o^\infty dK\ K^2\ \Phi_n^o(K)\ \frac{\sin(Kr)}{Kr} . \tag{8}$$

The modified von Karman spectrum is commonly used for Φ_n^o

$$\Phi_n^o(K) = \frac{\alpha e^{-K^2/K_m^2}}{(1 + K^2 L_o^2)^{11/6}}$$

$$K_m = 5.92/\ell_o \tag{9}$$

$$\alpha = \frac{L_o^3}{\pi^{3/2}} \cdot \frac{\Gamma(11/6)}{\Gamma(1/3)}$$

where α is a constant chosen so that $B_n^o(0) = 1$ and ℓ_o is the inner scale of turbulence. The von Karman spectrum appears to be adequate under conditions where the low frequency behavior of the spectrum is unimporant. However, the random path variations are predominantly influenced by refractive index perturbations in the spectral input range ($K \leq 2\pi/L_o$). Therefore, our results will be developed in terms of an arbitrary Φ_n^o so that the effects of different spectra can be studied. Substituting (8) in (7) and carring out the ρ integration gives

$$B_{\Delta L}(d) = 16\pi^2 \int_o^L d\xi\ B_n^\nu(\xi) \int_o^\infty dK\ K\Phi_n^o(K)\ J_o(Kd). \tag{10}$$

Another statistic of interest is the structure function for the path deviation. It is defined as the mean-square path difference and can be written in terms of $B_{\Delta L}$

$$D_{\Delta L}(d) = 2[B_{\Delta L}(0) - B_{\Delta L}(d)] = 32\pi^2 \int_o^L d\xi\ B_n^\nu(\xi) \int_o^\infty dK\ K\Phi_n^o(K)\ [1 - J_o(Kd)] . \tag{11}$$

When the path separation is small, the structure function is not sensitive to the low frequency behavior of Φ_n^o.

Similar expressions can be derived for angular path separations. Noting the geometry in Figure 1 and substituting (4) in (3) we obtain

$$B_{\Delta L}(\phi) = 4 \int_o^L dr_1 \int_o^L dr_2 B_n^\nu \left[\frac{(r_2+r_1)}{2} \cos(\phi/2)\right] B_n^o[((r_1-r_2)^2\cos^2(\phi/2) + (r_1+r_2)^2\sin^2(\phi/2))^{\frac{1}{2}}]. \tag{12}$$

Equation (12) was derived from (4) by assuming that B_n^ν is a function of the average of the projections of $\underline{r}_1$ and $\underline{r}_2$ onto the bisector of the angle ϕ. By making the change of variables

$$\begin{aligned} \frac{(r_1+r_2)}{2}\cos(\phi/2) &= \xi \\ (r_1-r_2)\cos(\phi/2) &= \rho \end{aligned} \tag{13}$$

and extending the ρ integration to infinity we have

$$B_{\Delta L}(\phi) = \frac{8}{\cos^2(\phi/2)} \int_o^L d\xi\, B_n^\nu(\xi) \int_o^\infty d\rho\, B_n^o[(\rho^2 + 4\xi^2\tan^2(\phi/2))^{\frac{1}{2}}]. \tag{14}$$

It is most convenient to write the covariance in terms of the refractivity spectrum. Substituting (8) in (14) and integrating over ρ gives

$$B_{\Delta L}(\phi) = \frac{16\pi^2}{\cos^2(\phi/2)} \int_o^\infty dK\, K\Phi_n^o(K) \int_o^L d\xi\, B_n^\nu(\xi)\, J_o[2K\xi\tan(\phi/2)]. \tag{15}$$

The structure function for the path deviation is

$$D_{\Delta L}(\phi) = 32\pi^2 \int_o^\infty dK\, K\Phi_n^o(K) \int_o^L d\xi\, B_n^\nu(\xi) \left[1 - \frac{J_o[2K\xi\tan(\phi/2)]}{\cos^2(\phi/2)}\right]. \tag{16}$$

The path deviation statistics for both parallel and angular path separations are summarized in Table I. These statistics were derived assuming that the refractive index correlation length L_o was much smaller than the total path length L. In this case the path deviation given in equation (1) is the sum of many statistically independent values of the refractive index. The central limit theorem can be used to argue that ΔL is Gaussian distributed. Thus, the correlation functions in Table I provide a complete statistical description of the Gaussian random variable ΔL for the path geometries considered. In the following sections these statistics will be evaluated for typical atmospheric parameters.

TABLE I

Path Deviation Statistics

Parallel Path

Covariance $$B_{\Delta L}(d) = 16\pi^2 \int_0^L d\xi\, B_n^{\nu}(\xi) \int_0^{\infty} dK K \Phi_n^{o}(K)\, J_o(Kd)$$

Structure Function $$D_{\Delta L}(d) = 32\pi^2 \int_0^L d\xi\, B_n^{\nu}(\xi) \int_0^{\infty} dK K \Phi_n^{o}(K) [1 - J_o(Kd)]$$

Angular Path

Covariance $$B_{\Delta L}(\phi) = \frac{16\pi^2}{\cos^2(\phi/2)} \int_0^{\infty} dK K \Phi_n^{o}(K) \int_0^L d\xi\, B_n^{\nu}(\xi)\, J_o[2K\xi \tan(\phi/2)]$$

Structure Function $$D_{\Delta L}(\phi) = 32\pi^2 \int_0^{\infty} dK K \Phi_n^{o}(K) \int_0^L d\xi\, B_n^{\nu}(\xi) \left[1 - \frac{J_o(2K\xi \tan(\phi/2))}{\cos^2(\phi/2)}\right]$$

2.2 RMS Path Deviation and Correlation Function

The mean square path deviation can be calculated using the covariance functions by setting d or ϕ equal to zero in (10) or (15)

$$\langle \Delta L^2 \rangle = 16\pi^2 \int_0^L d\xi \; B_n^{\nu}(\xi) \int_0^{\infty} dK \; K \Phi_n^{o}(K). \tag{17}$$

The refractive index variance, B_n^{ν}, is related to the turbulence structure parameter [2]

$$B_n^{\nu}(r) = 0.033 C_n^2(r) \frac{\pi^{3/2}\Gamma(1/3)}{\Gamma(11/6)} L_o^{2/3} = 0.523 \; C_n^2(r) L_o^{2/3}. \tag{18}$$

It is convenient to write the path deviation in terms of the structure parameter at the ranging site and an effective path length, L_e, defined as

$$L_e = \frac{1}{C_n^2(0)} \int_0^L d\xi \; C_n^2(\xi). \tag{19}$$

The mean-square path deviation for the von Karman spectrum (eq. (9)) is

$$\langle \Delta L^2 \rangle = 0.033 \; C_n^2(o) \frac{48\pi^2}{5} L_o^{5/3} L_e = 3.127 \; C_n^2(o) L_o^{5/3} L_e \tag{20}$$

The rms path deviation is plotted in Figures 2 and 3 as a function of C_n^2 for several values of L_e and L_o.

For horizontal paths the structure parameter will be essentially constant so that L_e is equal to the average path length L. Measurements by Bufton [3,4] have shown that turbulence exhibits a layered structure as a function of altitude. Except for a sharp peak near the tropopause, the structure parameter also exhibits an overall decay with increasing altitude (Figures 4 and 5). This decay roughly follows an exponential model [4-6]

$$C_n^2(h) = C_n^2(o) e^{-h/h_s} \tag{21}$$

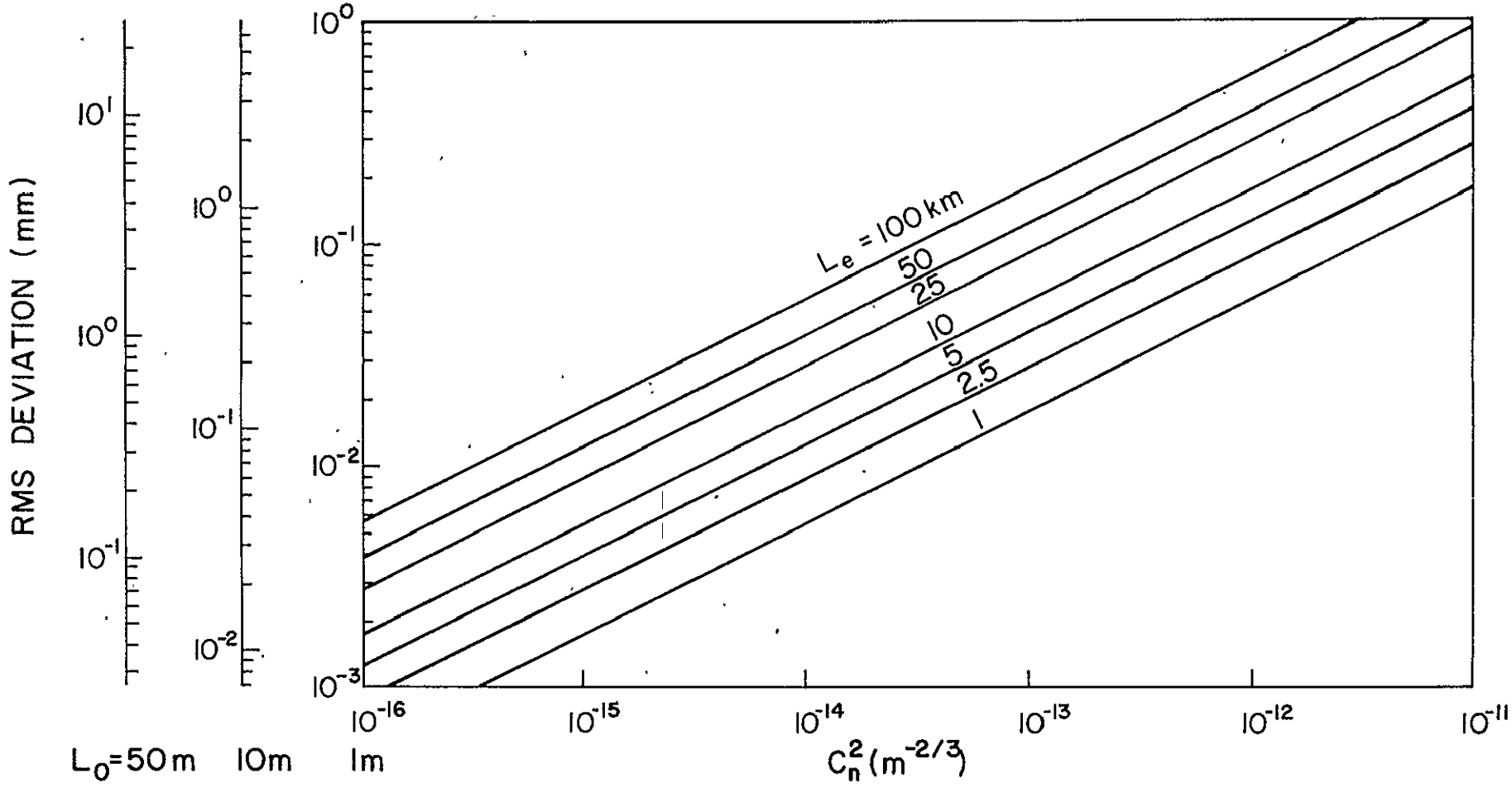

Figure 2. Rms path deviation given by eq. (20) for the von Karman spectrum. C_n^2 is the refractive index structure constant, L_o is the outer scale of turbulence and L_e is the effective path length in turbulence defined by eq. (19).

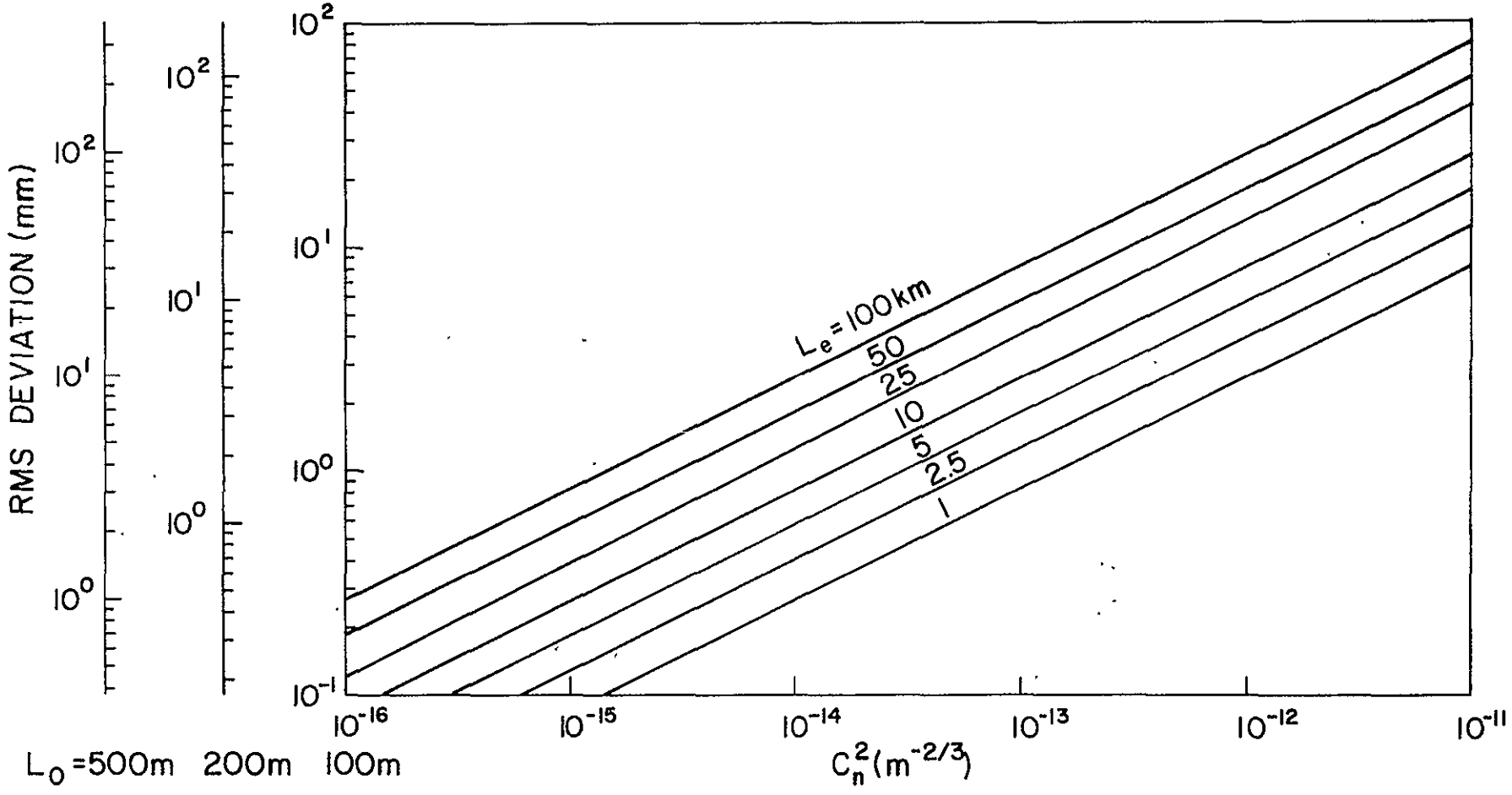

Figure 3. Rms path deviation given by eq. (20) for the von Karman spectrum. C_n^2 is the refractive index structure constant, L_o is the outer scale of turbulence and L_e is the effective path length in turbulence defined by eq. (19).

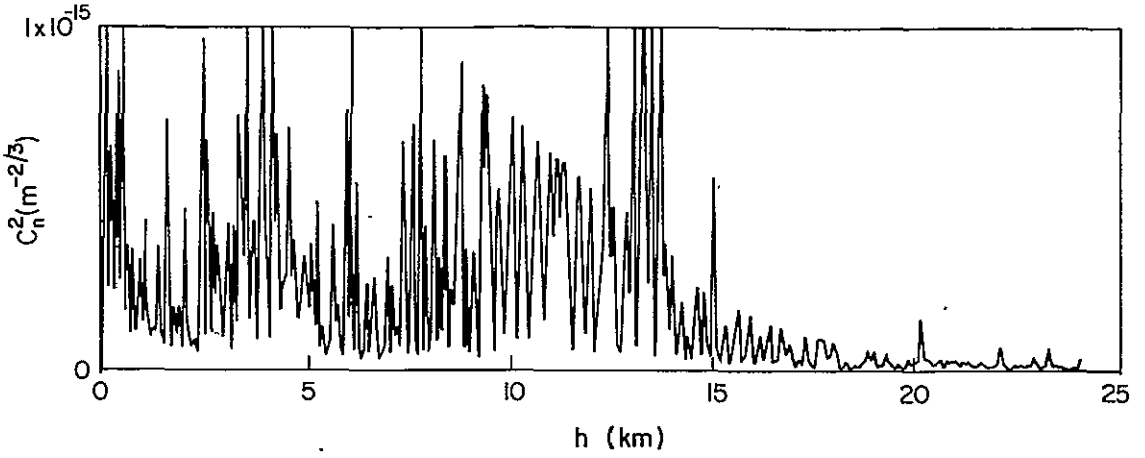

Figure 4. Measured dependence of C_n^2 on altitude. Figure is from Bufton's report, ref. [3].

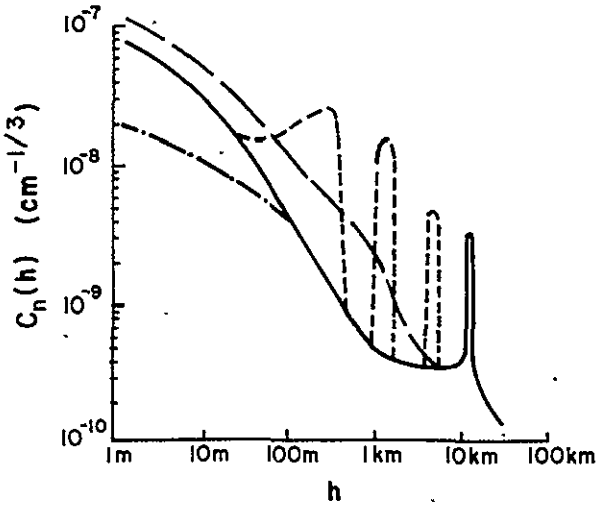

Figure 5. Hufangel's updated model for $C_n(h)$: ---, sunny day; ——, clear night; .-.-.-, dawn-dusk minimum; ..., disturbed layers. Local ground is assumed level and not on a mountain top. Figure is from Brookner's paper, ref. [5].

where h_s is the atmospheric scale height and h is the altitude. h_s is typically on the order of 2 to 5 Km. Then for satellite ranging the effective path length is

$$L_e = h_s \csc\psi \tag{22}$$

where ψ is the satellite elevation angle. L_o also varies with altitude. Values frequently used for L_o are about 100 meters or 1/3 to 1/5 the height above ground, whichever is less. For satellite ranging 100 meters should be used for the value of L_o.

The path deviations are predominantly influenced by the input range of the refractivity spectrum ($K \leq 2\pi/L_o$). To investigate the sensitivity of the path deviations to the form of Φ_n^o, the mean-square deviation was calculated for the following spectrum

$$\Phi_n^o(K) \propto \frac{e^{-K^2/K_m^2}}{(1+K^2L_o^2)^{\mu}} \tag{23}$$

$$\begin{aligned} \langle \Delta L^2 \rangle &= \frac{\Gamma(1/3)\Gamma(\mu-1)}{\Gamma(5/6)\Gamma(\mu-3/2)} \left[0.033 C_n^2(0)\ \frac{48\pi^2}{5}\ L_o^{5/3}\ L_e\right] \\ &= 7.42\ \frac{\Gamma(\mu-1)}{\Gamma(\mu-3/2)}\ C_n^2(0)\ L_o^{2/3} L_e\ . \end{aligned} \tag{24}$$

The ratio of the rms deviation for arbitrary μ to the deviation for $\mu = 11/6$ is plotted in Figure 6. As μ increases, more of the energy is concentrated in the low spatial frequencies for a fixed value of the refractive index variance. This effectively lengthens the tail of the refractive index covariance function which increases the rms deviation.

The parallel path correlation function can easily be calculated by substituting (23) into (10) and integrating over K. If inner scale effects are neglected (i.e. let $K_m = \infty$ in (23)) the correlation function can be evaluated in closed form

$$R_{\Delta L}(d) = B_{\Delta L}(d)/B_{\Delta L}(0) = \frac{2^{2-\mu}}{\Gamma(\mu-1)}\ \left(\frac{d}{L_o}\right)^{\mu-1}\ K_{\mu-1}\ \left(\frac{d}{L_o}\right) \tag{25}$$

where $K_{\mu-1}$ is a modified Bessel function.

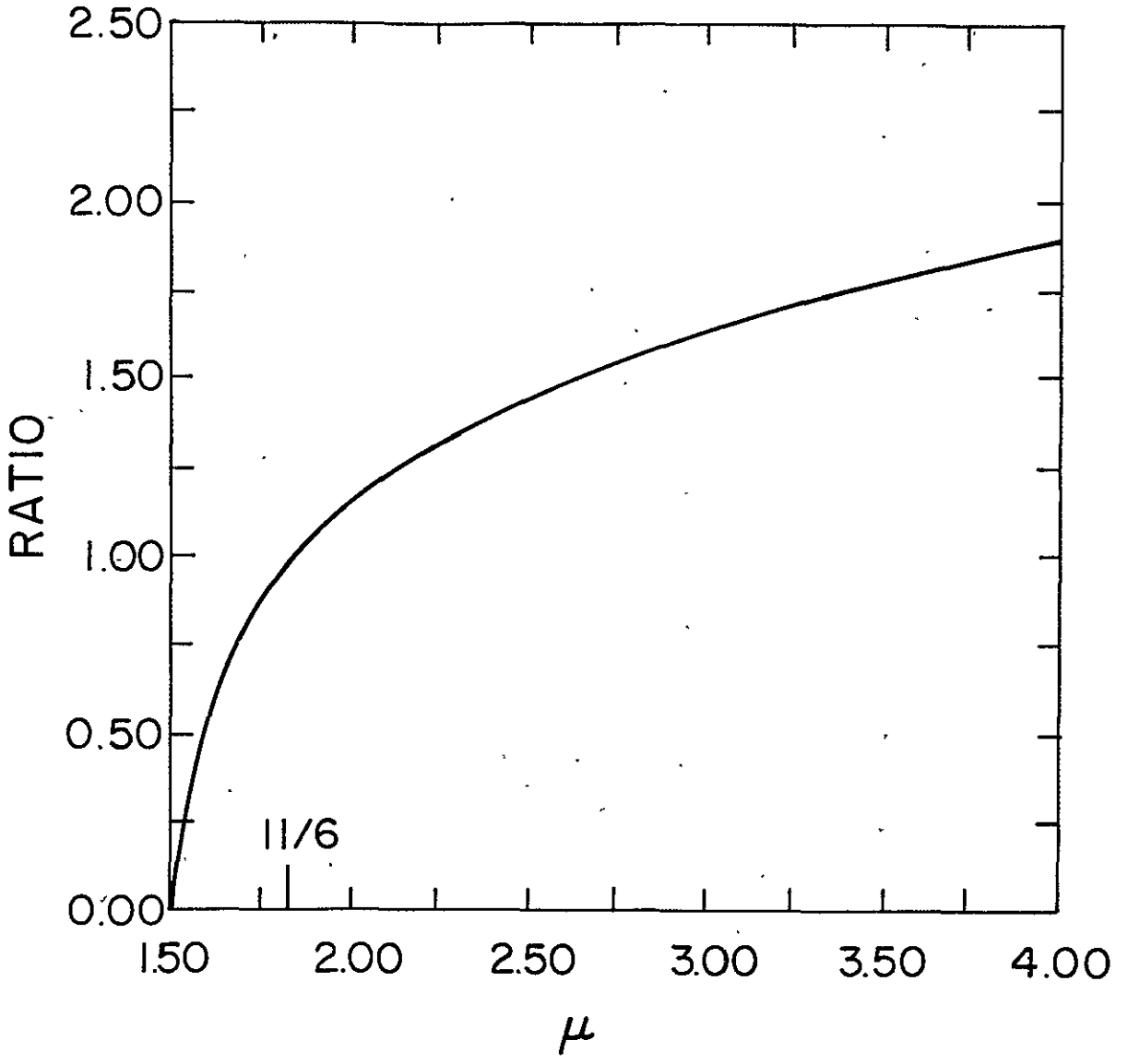

Figure 6. Ratio of the rms deviation calculated for the spectrum given in eq. (23) to the rms deviation calculated for the von Karman spectrum ($\mu = 11/6$).

The correlation functions are plotted in Figure 7 for several values of μ. When μ increases, the correlation tails increase as expected. The deviations on the two paths are essentially uncorrelated when the separation is on the order of L_o. The effects of the inner scale of turbulence are illustrated in Figure 8 where the correlation function is plotted for $\mu = 11/6$ for several values of $K_m L_o$. $K_m L_o$ is typically greater than 10^3 in the atmosphere so that inner scale effects can be neglected.

The angular path covariance function is more difficult to evaluate because it depends on the detailed behavior of the atmospheric structure parameter. For satellite ranging we will use the exponential model for C_n^2 given in (21). Brookner [5] has proposed a more complicated form of this model which includes a component to describe the tropopause contribution. Unfortunately the use of his model leads to considerable mathematical difficulties in calculating the angular correlation function. For this reason we will use the simpler model given in (21) which does give a fairly accurate description of C_n^2 [4,5]. In the following section Brookner's model is used to study the path structure function and is compared with the model in (21).

Using (21) the angular covariance function is given by

$$B_{\Delta L}(\phi) = \frac{C_n^2(0) h_s}{\cos^2(\phi/2)} \int_0^\infty dK\, K \Phi_n^o(K)\, [1 + K^2 \rho_s^2 \tan^2(\phi/2)]^{-\frac{1}{2}} \tag{26}$$

where

$$\rho_s = 2h_s \csc(\psi+\phi/2). \tag{27}$$

ψ is the initial elevation angle of the satellite (See Figure 1).

If the spectra given in equation (23) are used, the angular correlation can be written in terms of a hypergeometric function [7]

$$R_{\Delta L}(\phi) = \frac{B_{\Delta L}(\phi)}{B_{\Delta L}(0)} = \frac{1}{\cos^2(\phi/2)} \frac{(\mu-1)}{(\mu-1/2)} \, {}_2F_1(\tfrac{1}{2},\, 1,\, \mu+\tfrac{1}{2},\, 1 - \frac{\rho_s^2}{L_o^2}\tan^2(\phi/2)). \tag{28}$$

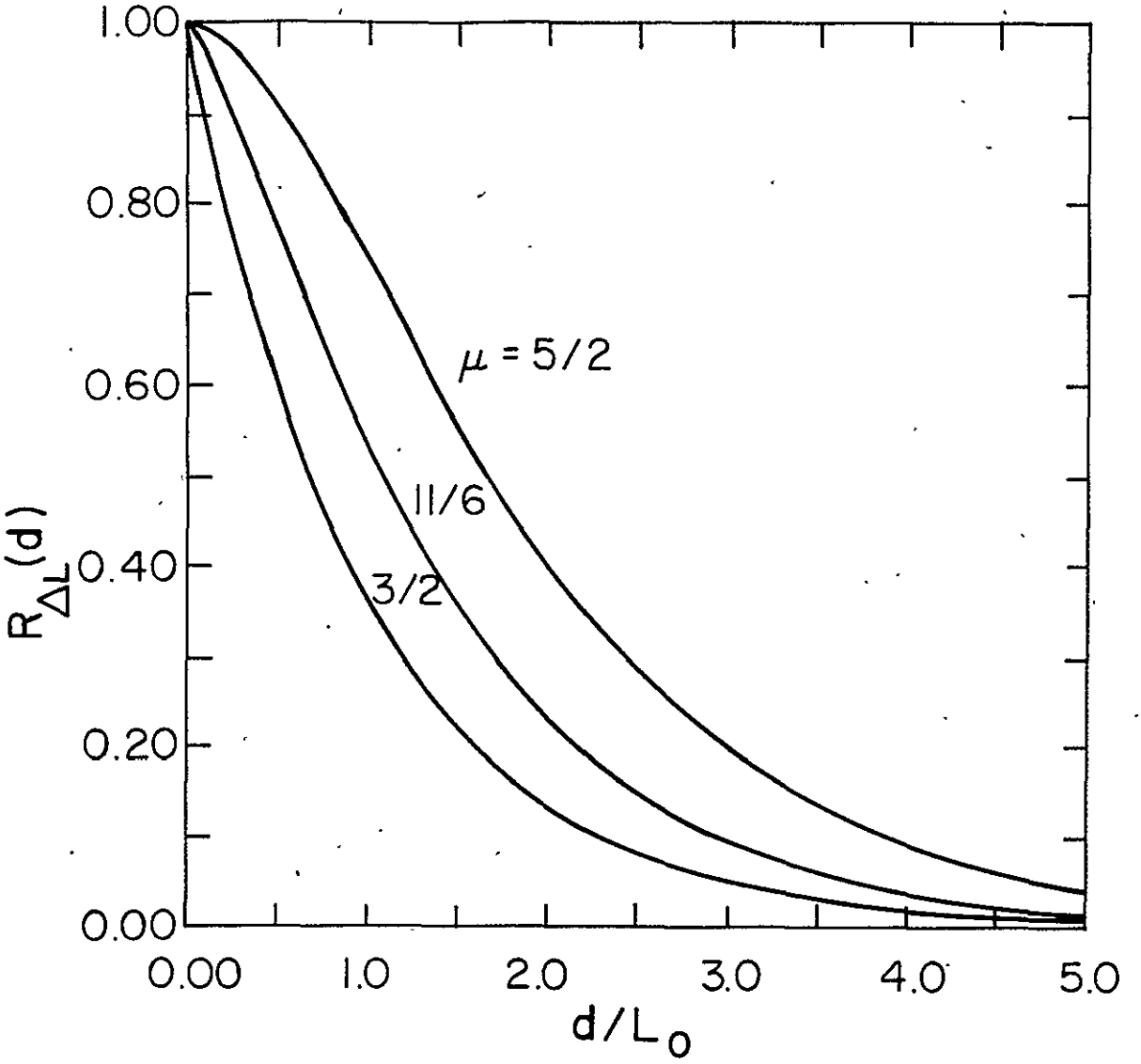

Figure 7. Parallel path correlation function for the spectral model in eq. (23). L_o is the outer scale of turbulence.

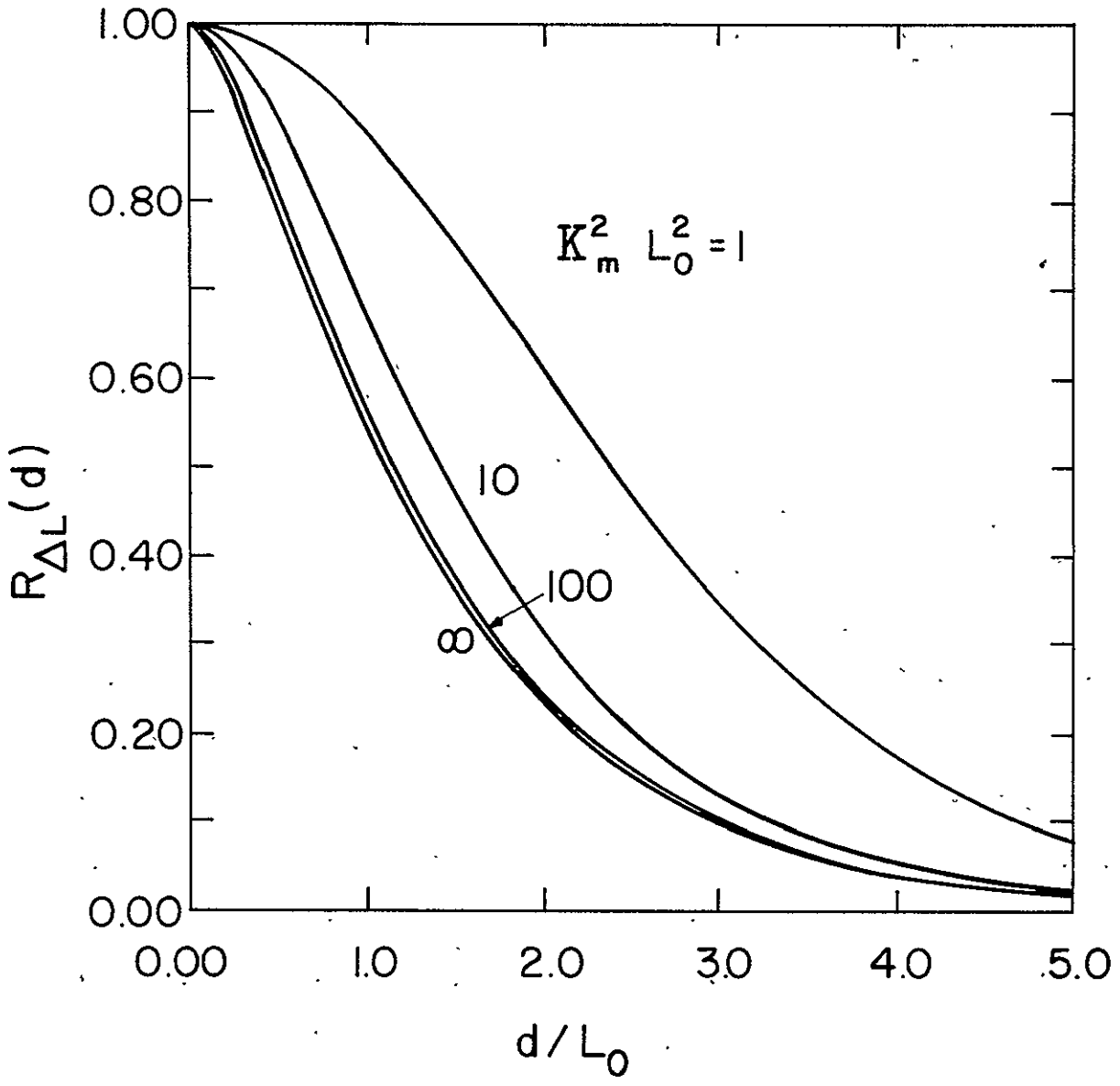

Figure 8. Parallel path correlation function for the von Karman spectrum ($\mu = 11/6$).

The path deviations are essentially uncorrelated when

$$\phi \simeq 2\tan^{-1}\left(\frac{L_o \sin\psi}{2h_s}\right) \simeq \frac{L_o \sin\psi}{h_s} = \phi_s . \tag{29}$$

The correlation angle ϕ_s is at most only a few degrees. When ϕ is on the order of or less than ϕ_s, the cosine factor in (28) can be set equal to one and the tangent approximated by the first term in its Taylor series expansion. In this case the angular correlation function becomes

$$R_{\Delta L}(\phi) = \frac{(\mu-1)}{(\mu-\frac{1}{2})}\, {}_2F_1\left(\tfrac{1}{2},\ 1,\ \mu+\tfrac{1}{2},\ 1-\phi^2/\phi_s^2\right) \tag{30}$$

$$\phi_s = \frac{L_o \sin\psi}{h_s}$$

The correlation functions given by (30) are plotted in Figure 9 for μ=3/2, 11/6, and 5/2. When μ increases the correlation tails also increases.

It should be pointed out that the path fluctuations on the satellite-earth path are nonstationary. Because the mean-square path deviations depend on the satellite elevation angle ψ (see (20) and (22)), the rms-path deviations will change as the satellite passes over the ranging site. The correlation function also depends on the satellite position since ρ_s and ϕ_o are functions of ψ. The path deviations decorrelate within a few degrees of angular separation. In the region of small ϕ, ρ_s will be essentially constant so that the effects of nonstationarity on the correlation function are negligble. For large ϕ ($>10^o$), the nonstationary effects must be considered by using equations (26) and (27) or (28) to calculate the correlation.

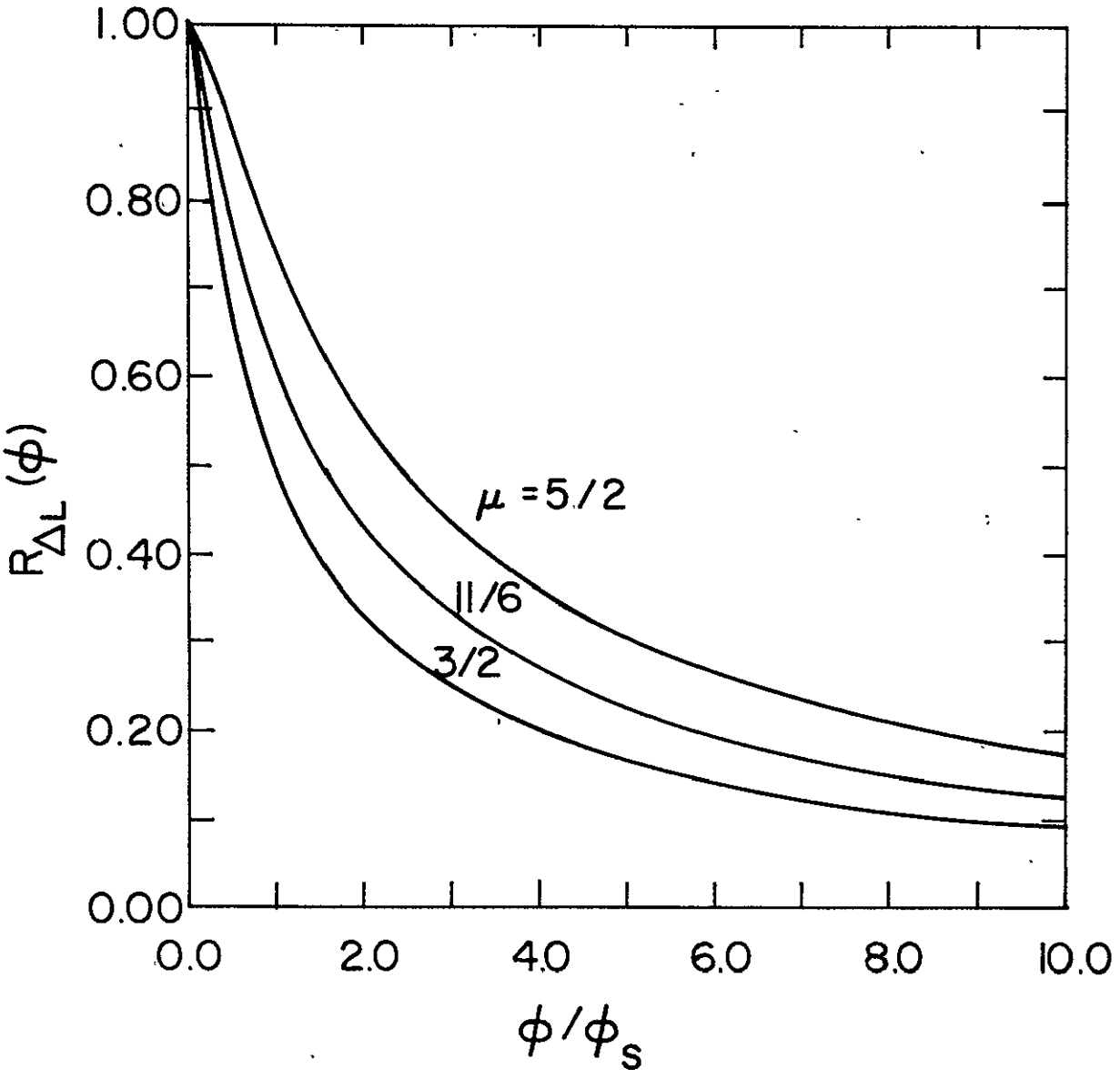

Figure 9. Angular path correlation function for the spectral model in eq. (23). ϕ_s is the correlation angle defined in eq. (30).

2.3 Structure Functions

The structure functions can be evaluated directly from the covariance by using the relation in equation (11). In this section we will compare the structure functions calculated using the von Karman spectrum with functions calculated using a new spectral model proposed by Greenwood and Tarazano [8]. The new model was derived empirically from atmospheric microtemperature measurements by varying parameters until a best fit to the temperature structure function data was obtained. Greenwood and Tarazano's (G-T) proposed spectrum is given by

$$\Phi_n^o(K) \propto (K^2 L_o^2 + K L_o)^{-11/6}. \tag{32}$$

It is plotted in Figure 10 along with the von Karman spectrum.

It is most convenient to calculate the normalized structure function because of its relationship to the correlation functions

$$\frac{D_{\Delta L}(d)}{D_{\Delta L}(\infty)} = 1 - R_{\Delta L}(d). \tag{33}$$

When d is small compared to the correlation length, the structure function is relatively insensitive to the low frequency behavior of the refractivity spectrum. In this region the structure function yields detailed information about the behavior of the main lobe of the correlation function. This information can be used to describe angle-of-arrival fluctuations and path variations across the receiving telescope aperture. In multicolored ranging systems, each frequency will traverse a slightly different path to and from the target because of dispersion in the atmosphere. The path fluctuations at each frequency will also be slightly different. The structure functions can be used to estimate these differences so that their effects on ranging accuracy of multicolored systems can be analyzed.

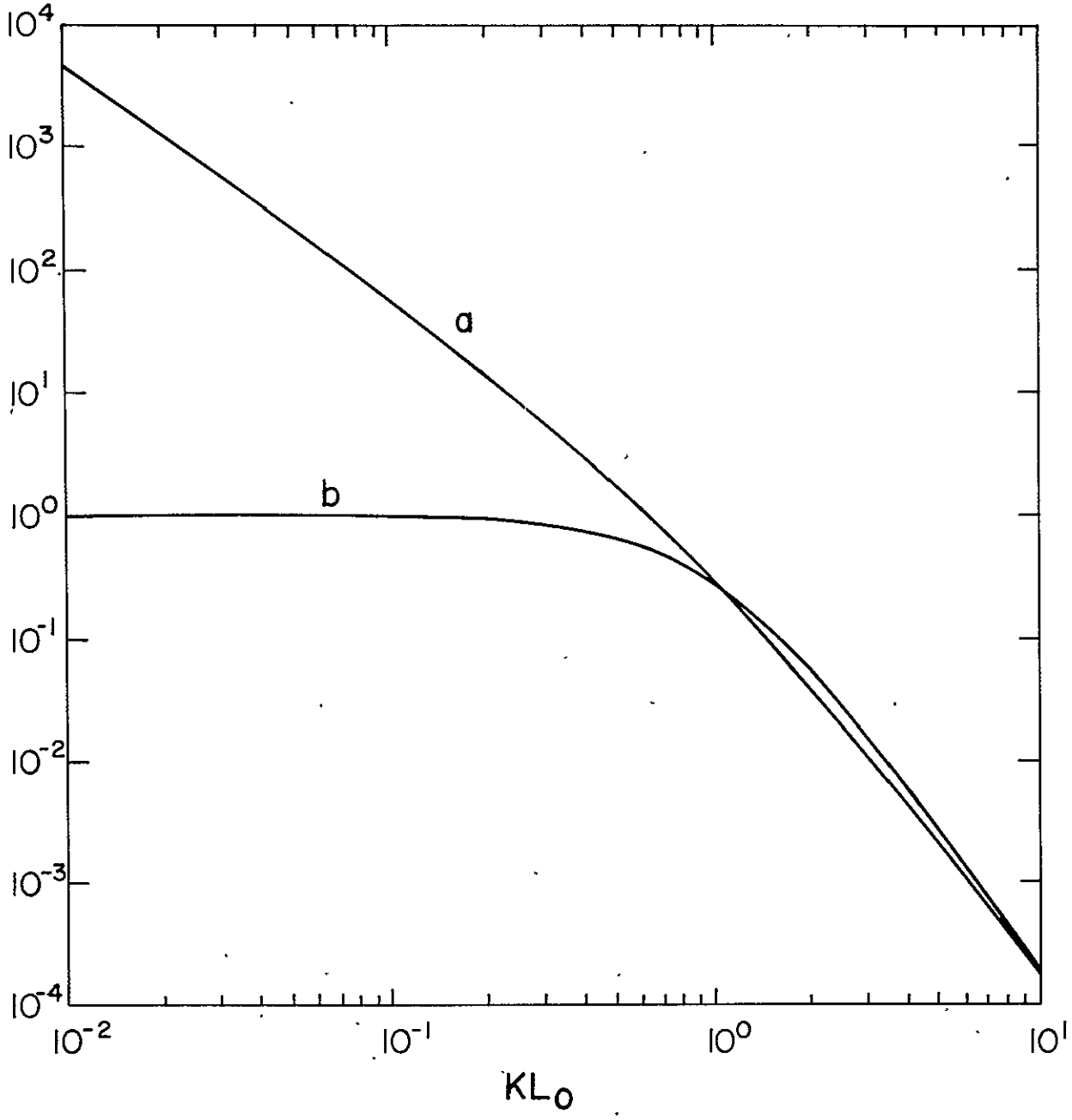

Figure 10. (a) Spectral model proposed by Greenwood and Tarazano [8], eq. (32) (b) The von Karman spectral model, eq. (9).

Using the von Karman spectrum the parallel-path structure function is given by

$$\frac{D_{\Delta L}(d)}{D_{\Delta L}(\infty)} = 1 - \frac{2^{1/6}}{\Gamma(5/6)} \left(\frac{d}{L_o}\right)^{5/6} K_{5/6}\left(\frac{d}{L_o}\right). \tag{34}$$

The asymptotic behavior for d small with respect to L_o is

$$\frac{D_{\Delta L}(d<<L_o)}{D_{\Delta L}(\infty)} \simeq \frac{\Gamma(1/6)}{2^{5/3}\Gamma(11/6)} \left(\frac{d}{L_o}\right)^{5/3} = 1.864\left(\frac{d}{L_o}\right)^{5/3}. \tag{35}$$

When $d >> L_o$ the asympototte is of course 1. The intersection of $D_{\Delta L}(d << L_o)$ and $D_{\Delta L}(d << L_o)$ is at

$$d = 0.688L_o. \tag{36}$$

The structure function is plotted versus d/L_o in Figure 11.

When the G-T model spectrum is used, the structure function cannot be expressed as simply as before. Following Greenwood and Tarazano's [8] approach we write $D_{\Delta L}$ in terms of confluent hypergeometric functions

$$\frac{D_{\Delta L}(d)}{D_{\Delta L}(\infty)} = 1 - \frac{\frac{1}{\pi}\int_0^{\pi} d\Theta\ U(1/6, -2/3, -i\frac{d}{L_o}\cos\Theta)}{U(1/6, -2/3, 0)} \tag{37}$$

The derivation of (37) is detailed in Appendix A where the first term of the power series expansion in $\frac{d}{L_o}$ is also evaluated. The small d asymptote is given by

$$\frac{D_{\Delta L}(d << L_o)}{D_{\Delta L}(\infty)} \simeq 0.2093\left(\frac{d}{L_o}\right)^{5/3} \tag{38}$$

and the intersection of $D_{\Delta L}(d << L_o)$ and $D_{\Delta L}(d >> L_o)$ is at

$$d = 2.56L_o. \tag{39}$$

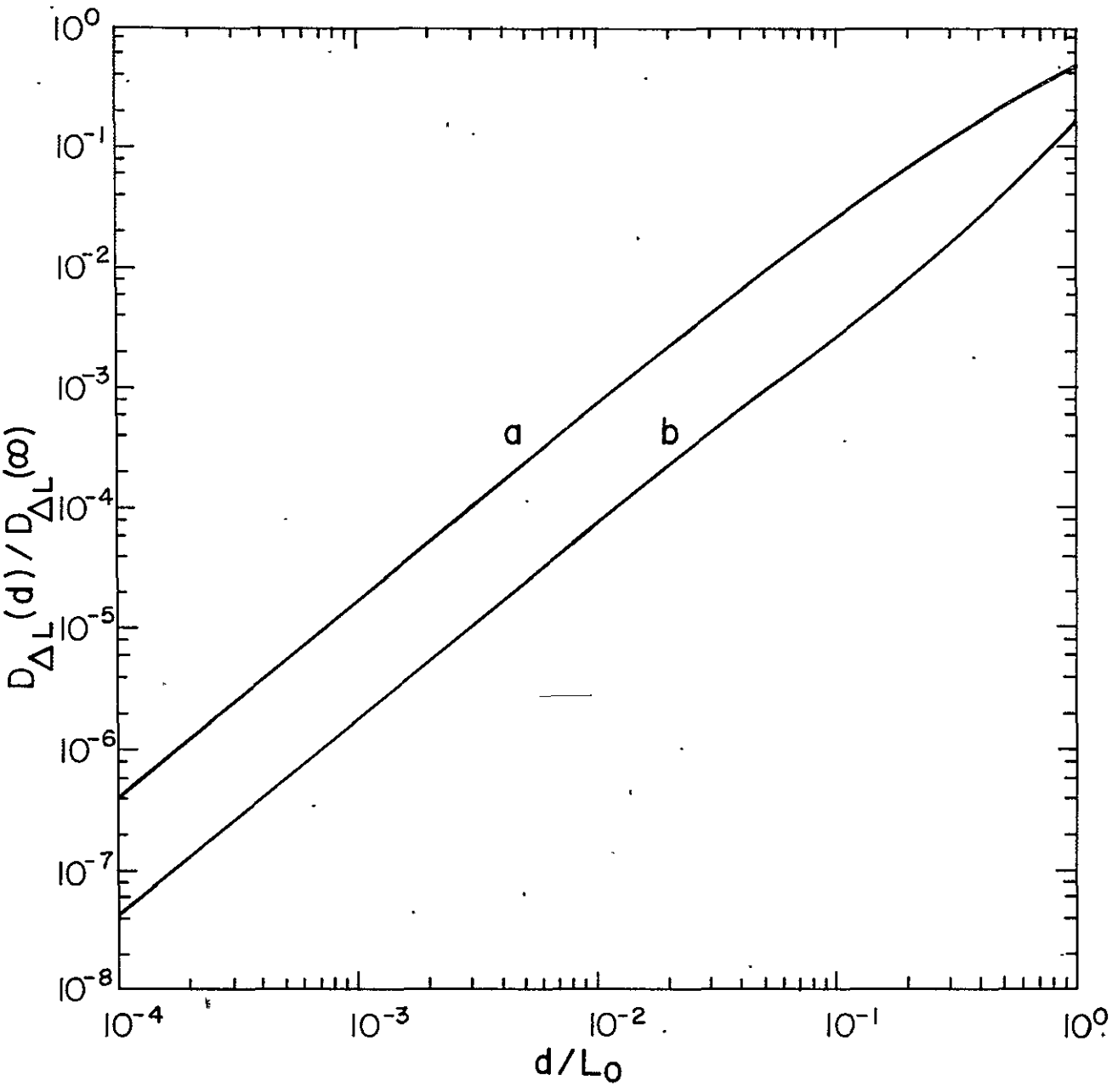

Figure 11. Parallel path structure functions. (a) von Karman spectrum, eq. (34). (b) Greenwood and Tarazano spectrum, eq. (37).

Equations (38) and (39) are considerably different from the corresponding results for the von Karman spectrum ((35) and (36)). This is illustrated in Figure 11 where the structure functions for both the von Karman and the G-T spectra are plotted. The structure function increases much more slowly with the G-T model. This indicates that the corresponding correlation function has a much longer tail. The effect results because there is more energy in input range of the G-T model (see Figure 10).

These results are interesting because of their implications regarding the mean-square path deviations. The mean square deviation calculated using the G-T model is given by

$$\langle \Delta L^2 \rangle_{G\text{-}T} = \frac{2\pi^{\frac{1}{2}}\Gamma(1/3)}{\Gamma(5/6)} \left[0.033 C_n^2(0) \frac{48\pi^2}{5} L_o^{5/3} L_e \right] \tag{40}$$

$$= 26.31\ C_n^2(0)\ L_o^{5/3}\ L_e$$

The rms deviation calculated for the G-T model is approximately 3 times greater than the corresponding results for the von Karman spectrum. Because the G-T model was derived emperically from actual atmospheric measurements we believe that (40) represents a more realistic value for the mean-square path deviations than the results obtained from the von Karman spectrum. The rms deviations for the G-T model can be obtained from Figures 2 and 3 simply by multiplying the values by

$$\left(\frac{2\pi^{\frac{1}{2}}\Gamma(1/3)}{\Gamma(5/6)} \right)^{\frac{1}{2}} \simeq 2.9 \tag{41}$$

The structure functions for the angular path depend on both the refractivity spectrum and the behavior of C_n^2. If C_n^2 is described by the exponential model given in (21), the structure function can easily be calculated from (30) with $\mu = 11/6$

$$\frac{D_{\Delta L}(\phi)}{D_{\Delta L}(\pi)} = 1 - \frac{5}{8}\,{}_2F_1(\tfrac{1}{2},\ 1,\ 7/3,\ 1 - \phi^2/\phi_s^2). \tag{42}$$

The small angle asymptote is

$$\frac{D_{\Delta L}(\phi << \phi_s)}{D_{\Delta L}(\pi)} \simeq \frac{\Gamma(1/6)\Gamma(4/3)}{\Gamma(\tfrac{1}{2})}\left(\frac{\phi}{\phi_s}\right)^{5/3} = 2.804\left(\frac{\phi}{\phi_s}\right)^{5/3} \tag{43}$$

and the intersection of $D_{\Delta L}(\phi << \phi_s)$ and $D_{\Delta L}(\phi >> \phi_s)$ is at

$$\phi = 0.539\ \phi_s. \tag{44}$$

Equation (42) is plotted in Figure (12).

When the G-T spectrum is used, the angular structure function can be derived from the parallel path structure function given by (37). The calculations are detailed in Appendix B and plotted in Figure 12 along with the corresponding results for the von Karman spectrum. The small ϕ asymptote is

$$\frac{D_{\Delta L}(\phi << \phi_s)}{D_{\Delta L}(\pi)} \simeq 0.315\ \left(\frac{\phi}{\phi_s}\right)^{5/3} \tag{45}$$

and the intersection of $D_{\Delta L}(\phi << \phi_s)$ and $D_{\Delta L}(\phi >> \phi_s)$ is at

$$\phi = 2.00\ \phi_s. \tag{46}$$

The angular structure functions also increase more slowly when the G-T model spectrum is used. These results imply that the path deviations do not decorrelate as rapidly as might be expected with the von Karman model.

Brookner [5] has proposed a more complicated version of the exponential model for the variations in C_n^2 with altitude

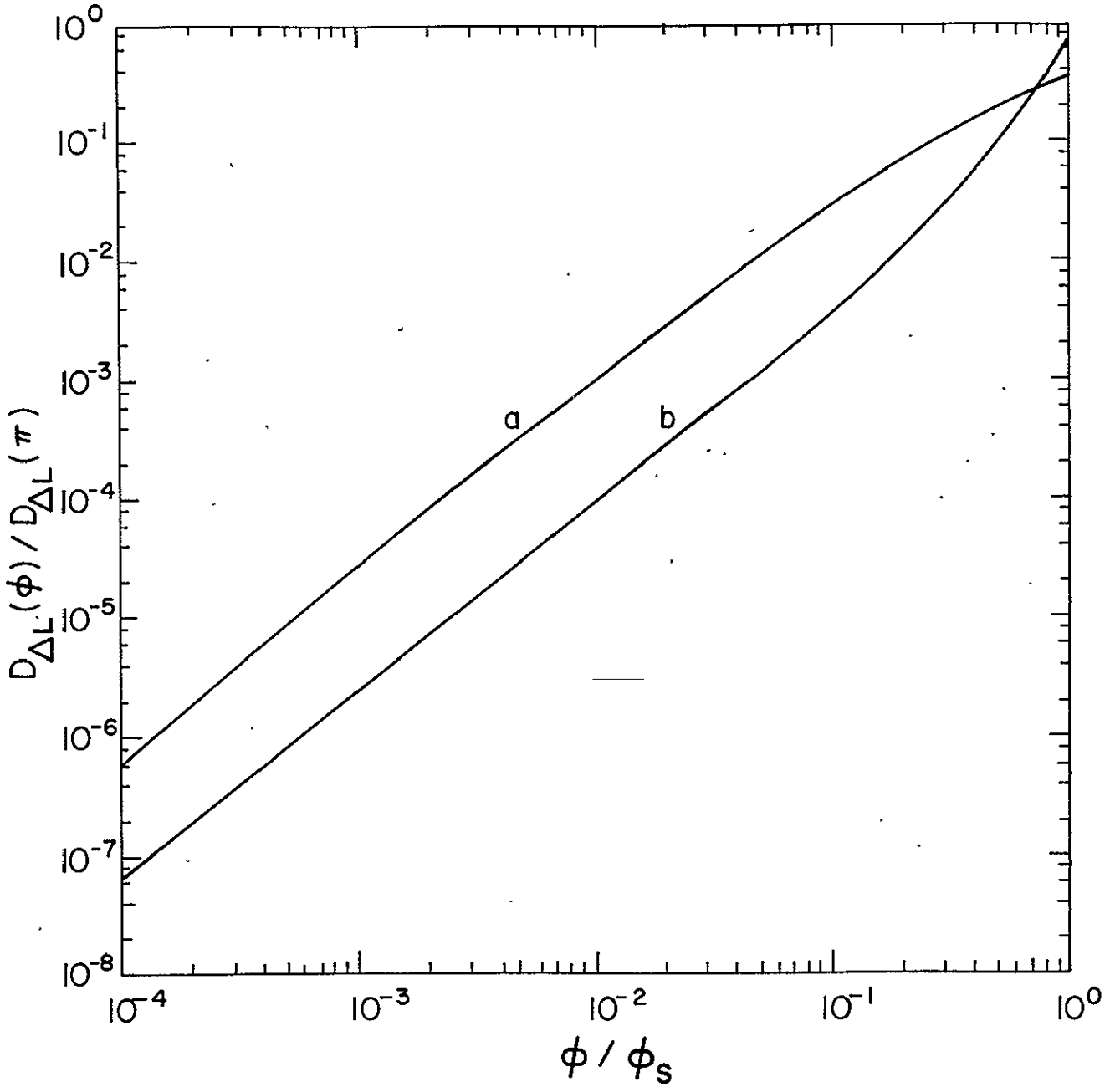

Figure 12. Angular path structure functions. (a) von Karman spectrum, eq. (42). (b) Greenwood and Tarazano spectrum, eq. (45).

$$C_n^2(h) = C_{no}^2\, h^{-b}\, e^{-h/h_s} + C_{nT}^+\, \delta(h-h_T) \tag{47}$$

h_s is the atmospheric scale height which in general is different from the h_s employed in (21). The parameter b is chosen depending on the conditions, and C_{no}^2 is specified so that $C_n^2(h)$ is in $m^{-2/3}$ when h is in meters. The second term in (47) is the tropoause contribution. h_T is the tropopause height and C_{nT}^+ is the integral of $C_n^2(h)$ under its peak at the tropopause. When b and C_{nT}^+ are zero, (47) reduces to the model given in (21). Brookner suggests a value of 320 m. for h_s and 12 km. for h_T. The model given by (21) requires h_s to be on the order of 3.5 km.

When Brookner's model is used, the covariance and structure function separate into two terms. To illustrate, the angular correlation function is derived in Appendix C for the von Karman spectrum using Brookner's model for $C_n^2(h)$

$$R_{\Delta L}(\phi) = \frac{C_n^+}{(C_n^+ + C_{nT}^+)}\, \beta_o\, {}_2F_1(\tfrac{1}{2}-b/2,\ 1-b/2,\ 7/3-b,\ 1-\phi^2/\phi_s^2) + \frac{C_{nT}^+}{(C_n^+ + C_{nT}^+)}\, \overline{\beta_1}\, (\phi/\phi_T)^{5/6} K_{5/6}(\phi/\phi_T)\,, \quad b<1 \tag{48}$$

where

$$\phi_s = \frac{L_o}{h_s}\sin\psi$$

$$\phi_T = \frac{L_o}{h_T}\sin\psi \tag{49}$$

and β_o and β_1 are constants defined in Appendix C. C_n^+ and C_{nT}^+ are the integrated contributions due to the lower atmosphere and tropopause respectively. In this case the path deviations are characterized by two distinct correlation angles. The tropopause correlation angle ϕ_T is generally much smaller than the lower atmosphere correlation angle ϕ_s. Consequently, there is an initial rapid decorrelation as ϕ

approaches ϕ_T. The correlation then saturates at a value approximately equal to $C_n^+/(C_n^+ + C_{nT}^+)$ until ϕ approaches ϕ_s. Then the correlation decays to zero as the deviations due to the lower atmosphere decorrelate.

This effect is nicely illustrated in Figures 13 and 14 where the correlation and structure functions are plotted. We have used the parameter values suggested by Brookner in reference [5]. The values were selected by Brookner to obtain a best fit of the model to data published by Hufnagel [9]. In all cases the initial decorrelation (increase of the structure function) is dominated by the tropopause contribution.

It should be pointed out that even Brookner's improved model is still an approximation at best. Bufton's [3, 4] data which was collected during the dawn-dusk minimum periods show a highly layered structure to the turbulence. Based upon the results from Brookner's model, we might expect the strongest layers to each have an associated correlation angle so that the structure functions would be even more complicated than those illustrated in Figures 13 and 14. The initial decorrelation will probably be determined by the highest layers near the tropopause.

The effects of turbulence on laser ranging systems will be most apparent on sunny days when the turbulence is strong. The G-T spectrum predicts rms deviations approaching a few centimeters (eq. (40) and (41) and Figure 3). In this case the lower atmosphere is the major source of the path deviations. Significant decorrelation will occur only when the separation approaches the lower atmosphere correlation angle ϕ_s while the initial decorrelation will still be determined by the tropopause (Figures 13 and 14).

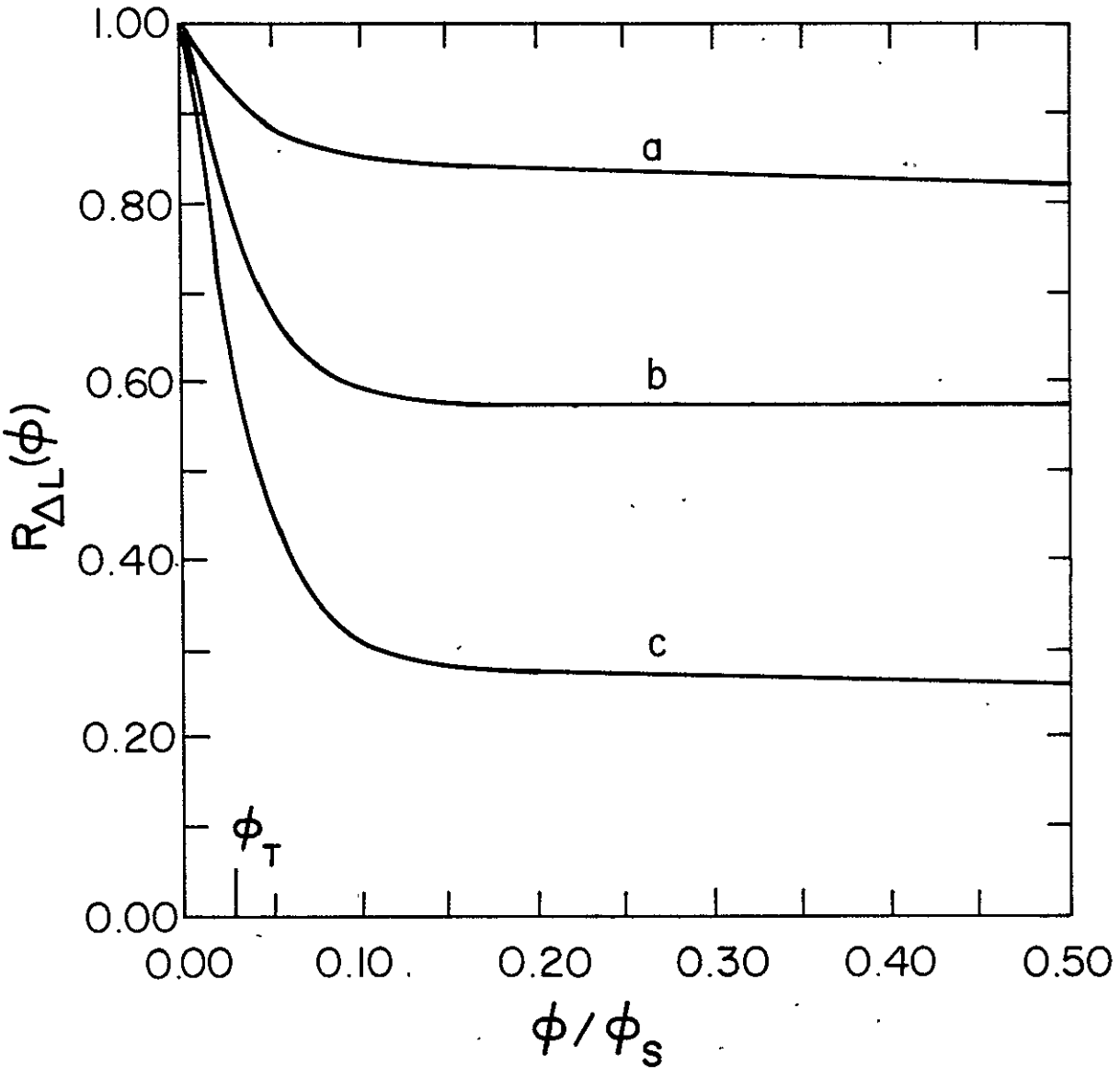

Figure 13. Angular path correlation function calculated using Brookner's [5] improved model for C_n^2 (h) given in eq. (47). (a) Sunny day. (b) Clear night. (c) Dawn-dusk minimums.

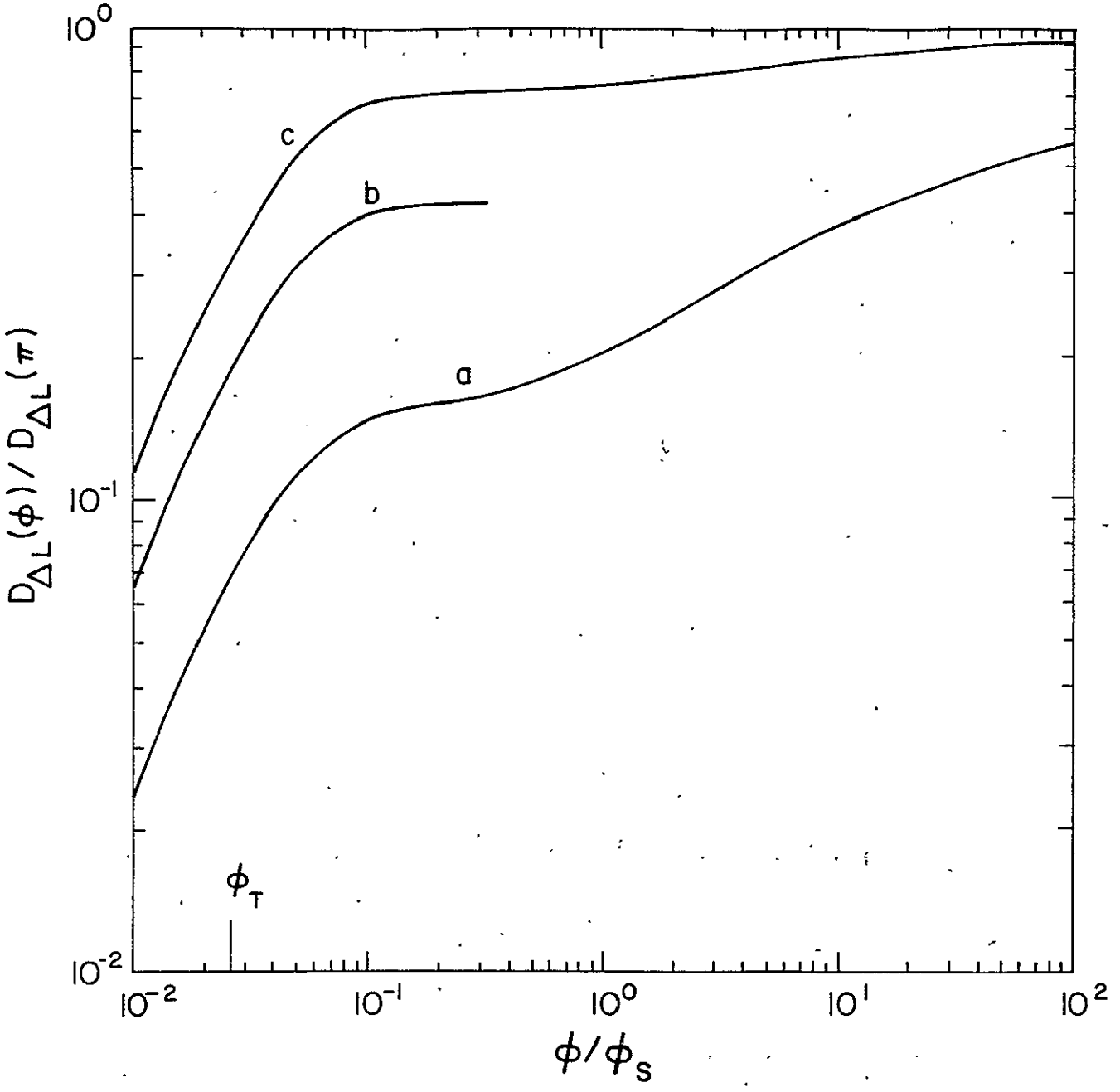

Figure 14-a. Angular path structure function calculated using Brookner's [5] improved model for C_n^2 (h) given in eq. (47). (a) Sunny day. (b) Clear night. (c) Dawn-dusk minimums.

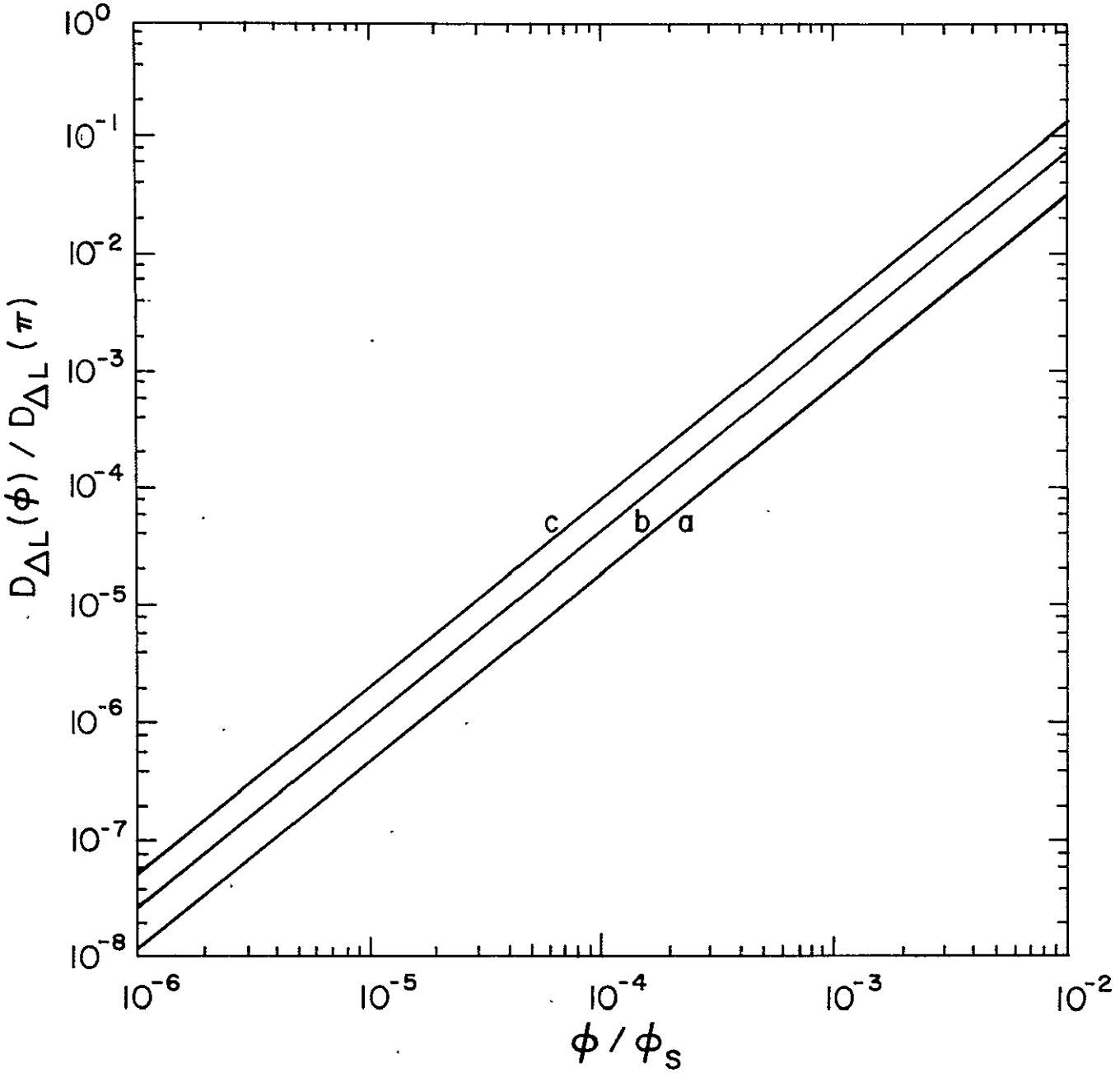

Figure 14-b. Angular path structure function calculated using Brookner's [5] improved model for C_n^2 (h) given in eq. (47). (a) Sunny day. (b) Clear night. (c) Dawn-dusk minimums.

3. EFFECTS OF PATHS FLUCTUATIONS ON RANGING ACCURACY

The statistical characteristics of random path length fluctuations were derived in the previous section. In this section the effects of path fluctuations on the accuracy of single color and two color ranging systems are examined.

3.1 Single Color Ranging Systems

The optical path length for a roundtrip between the ranging site and target is given by

$$L = \int_c d\underline{r}\, n_o(\underline{r}) + \int_c d\underline{r}\, n_1(\underline{r}) = \langle L \rangle + \Delta L \qquad (50)$$

$\langle L \rangle$ is the average path length which is determined by the average refractivity (n_o) along the ray path. ΔL is the instantaneous random path deviation caused by fluctuations in the refractive index (n_1). ΔL is Gaussian distributed and its statistics were derived in Section 2.

When a range measurement is made, L is the parameter that is actually measured. Formulas are available (e.g. ref. [10-12]) which can partially correct the measurements for the effects of the average atmospheric refraction. Since ΔL is random, it is not possible to correct the measurement for the effects of turbulence. ΔL represents a fundamental limit in the accuracy of single color ranging systems.

The rms value of ΔL was calculated in the previous section and plotted in Figures 2 and 3 for typical atmospheric parameters. Figures 2 and 3 are based on equation (20) which was derived for the von Karman spectrum. These results probably represent a conserative estimate for ΔL_{rms}. The rms deviation was also calculated using a new spectral model proposed by Greenwood and Tarazano [8]. The G-T model gives a value for ΔL_{rms} approximately 3 times larger than the results for the von Karman spectrum. Because the G-T model

was derived emperically from actual atmospheric measurements of the temperature structure function, we believe that it gives a more realistic value for the rms path deviations.

When the structure parameter follows the exponential model in (21) the effective path length in turbulence L_e is given by (22). L_o and h_s are on the order of 100 m and 3 km respectively. Under these conditions the rms path deviations can be up to a few centimeters when the satellite is at low elevation angles ($\sim 10^{o}$) and the turbulence is very strong ($C_n^2 \sim 10^{-13}$ $m^{-2/3}$). Under most conditions C_n^2 will be much weaker (10^{-15} $m^{-2/3}$) so that rms deviations will be a few millimeters or less.

It is possible to reduce the effects of the path deviations by averaging many different range measurements. The amount of reduction depends on the correlation between the path deviations on each measurement. If the path deviations are stationary and n measurements are averaged, the residual rms deviation is given by

$$\frac{1}{n} \left(\sum_{i=1}^{n} \sum_{j=1}^{n} \rho_{ij} \right)^{\frac{1}{2}} \Delta L_{rms} \tag{51}$$

where ΔL_{rms} is the deviation on a single measurement and ρ_{ij} is the correlation between the path deviations on i^{th} and j^{th} measurement. If the measurements are statistically independent, the rms deviation is reduced by the factor $1/\sqrt{n}$.

The path deviation correlation functions were derived in Section 2 (see Figures 7 and 9). For satellite ranging the path deviations decorrelate when the angular separation is on the order of $\phi_s = \frac{L_o}{h_s} \sin\psi$. The time required for the Lagoes satellite to move an angular distance ϕ_s is on the order of tens of seconds. Typical laser ranging systems are capable of

making many measurements within this time period. When the correlation between successive measurements is high, the summations in (51) can be approximated as integrals. To see this, let the angular velocity of the satellite as viewed from the ranging site be constant and denoted by ω. The averaging operation can be written as an integration

$$\Delta L_{avg} = \frac{1}{T}\int_0^T dt\ \Delta L(\phi=\psi+\omega t) \tag{52}$$

T is the length of the time interval over which the measurements are averaged and ψ is the satellite elevation angle on the first measurement at t=o. The mean square value of the integral is given by

$$\langle \Delta L_{avg}^2 \rangle = \frac{2}{T}\int_0^T dt\ (1-t/T) B_{\Delta L}(\phi = \omega t) \tag{53}$$

Equation (53) can be rewritten in terms of the refractive index spectrum

$$\langle \Delta L_{avg}^2 \rangle = \frac{64\pi^2}{\omega T}\int_0^\infty dK\ K\Phi_n^o(K)\int_0^L d\xi\ B_n^\nu(\xi)\int_0^{\tan(\omega T/2)} dx\left(1-\frac{2}{\omega T}(\tan^{-1}X)\right) J_o(2K\xi X). \tag{54}$$

(54) was derived by substituting (15) into (53) and making the change of variables $x = \tan(\omega t/2)$. Notice ωT is the total angle over which the measurements were averaged.

The ratio of ΔL_{rms} for the averaged measurements to ΔL_{rms} for a single measurement is plotted in Figure 15 as a function of ωT. The results were calculated using the angular correlation function given in (28) for μ = 3/2, 11/6 and 5/2. This corresponds to the spectral model given in (23) for Φ_n^o and the expontential model given in (21) for B_n^ν. There is suprisingly little reduction even when the measurements are averaged over 10 correlation angles. This is due primarily to the long tails on the angular correlation functions (see Figure 9). The effects of wind were not included in the derivation

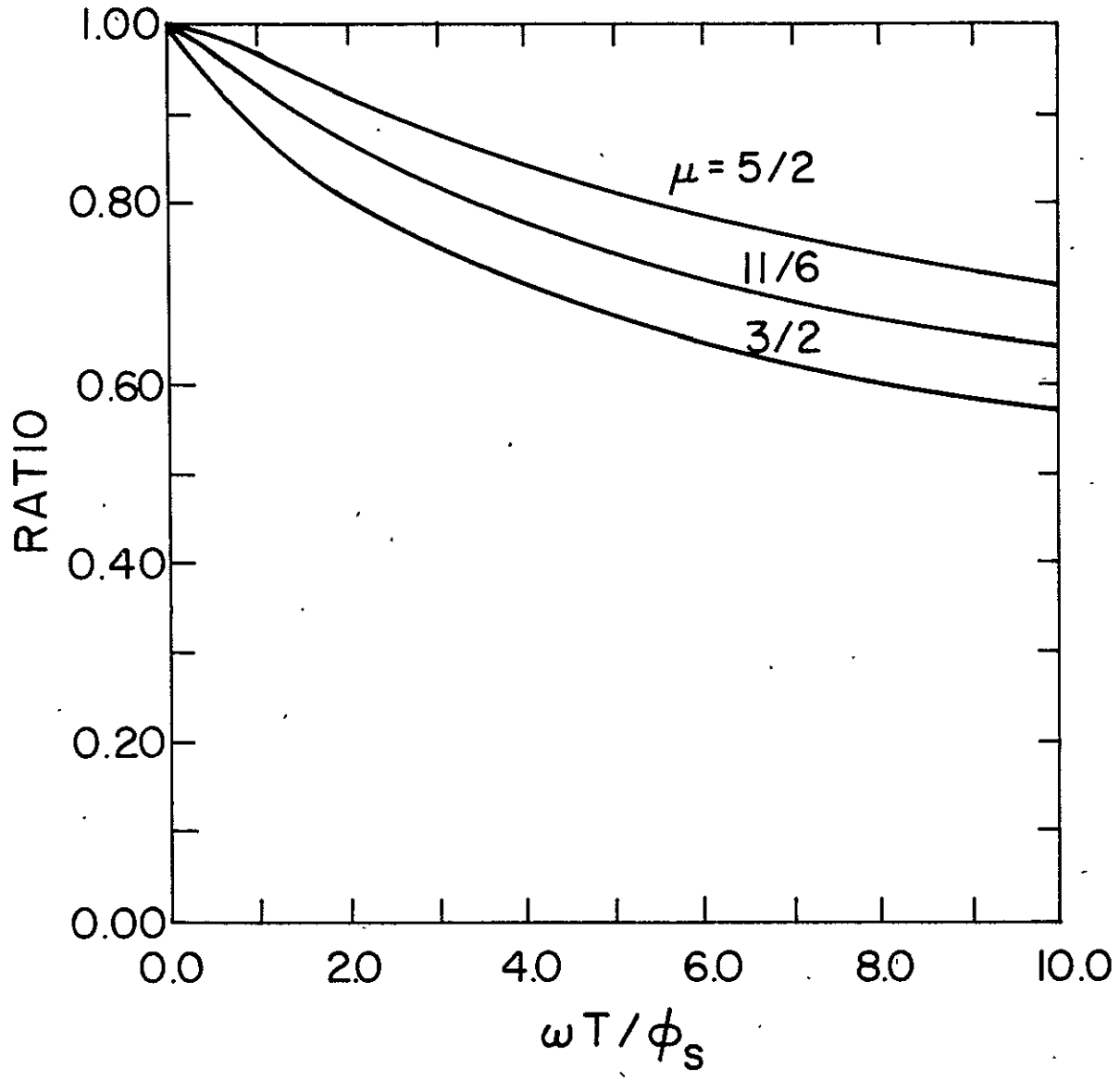

Figure 15. Ratio of the rms path deviation for time-averaged measurements to the rms deviation for a single measurement. ω is the angular velocity of the satellite as seen from the ranging site, T is the averaging time and ϕ_s is the correlation angle (eq. (30)). The results we calculated using the spectral model given by eq. (23).

of the correlation functions in the previous section. Wind motion transverse to the propagation path will tend to decorrelate the path deviations more rapidly when the wind velocity is in the direction opposite the satellite motion. When the wind velocity is in the same direction as the satellite motion, the path deviations tend to remain correlated much longer. Figure 15 was derived assuming no wind and probably represents an average of these two extreme cases. Wind motion will be important only when the transverse speed $V_\perp$ is large enough to blow a turbulent blob of size L_o across the propagation path during the integration time, i.e. if $T \gtrsim L_o/V_\perp$. The wind speed in the lower atmosphere is typically on the order of a few tens of meters per second. Therefore, the results in this section apply for integration times from a few seconds to about 1 minute.

Equations (52) and (54) can be simplified if we assume that the integration time is long compared to the correlation time (i.e. $\omega T >> \phi_s$). In this case t/T will be small over the important range of integration and can be neglected in (52). The upper limit on the T integration can be extended to π/ω since $B_{\Delta L}$ is negligible when $T >> \phi_s/\omega$

$$\langle \Delta L^2_{avg} \rangle \simeq \frac{1}{T} \int_0^{\pi/\omega} dt\, B_{\Delta L}(\phi=\omega t). \tag{55}$$

Similarly, if we neglect the dependence of B_n^ν on ϕ (B_n^ν is evaluated for the elevation angle $\psi + \phi/2$), the term $\frac{2}{\omega T} \tan^{-1} X$ can be neglected in (54) and the upper limit on the X integration can be extended to infinity

$$\langle \Delta L^2_{avg} \rangle \simeq \frac{32\pi^2}{\omega T} \int_0^\infty dK\, \Phi_n^o(K) \int_0^L d\xi\, \xi^{-1}\, B_n^\nu(\xi) \tag{56}$$

Equation (56) can be used to obtain estimates of the residual path deviations when the measurements are averaged over many correlation angles. However, since wind was also neglected in (56), the results still apply only for integration times less than about 1 minute.

Similar results can be obtained for horizontal propagation paths using the parallel path correlation functions. If the ranging site and target are stationary, the path separation d is replaced by $V_\perp t$ where $V_\perp$ is the transverse wind velocity. The wind velocity is assumed to be uniform along the propagation path. If the ranging site and target are moving in the same direction at identical speeds, $V_\perp$ is their transverse velocity. The mean square deviation of the averaged measurements is

$$\langle \Delta L^2_{avg} \rangle = \frac{32\pi^2}{T} \int_0^L d\xi \; B_n^\nu(\xi) \int_0^\infty dK K \Phi_n^o(K) \int_0^T dt (1-t/T) J_o(K V_\perp t). \tag{57}$$

When T is large compared to the correlation time $L_o/V_\perp$ (57) simplifies to

$$\langle \Delta L^2_{avg} \rangle \simeq \frac{32\pi^2}{V_\perp T} \int_0^L d\xi \; B_n^\nu(\xi) \int_0^\infty dK \; \Phi_n^o(K). \tag{58}$$

3.2 Two Color Ranging Systems

A significant improvement in ranging accuracy should be possible if two laser frequencies are employed instead of one. The difference between the refraction at different wavelengths can be used to eliminate, to a great extent, the effects of atmospheric refraction on the range measurements [13-15]. The technique entails measuring the range at two frequencies. The difference in range at the two frequencies is a measure of the refractive conditions existing over the propagation path at the instant the measurements were taken and can be used to improve the accuracy of the range measurements.

Because the two color system effectively measures conditions along the actual propagation path at a given instant, the system can also correct for the random path deviations caused by turbulence. However, dispersion and refractivity gradients transverse to the propagation path will cause the two color paths to separate slightly. Since the turbulence on the two paths will only be partially correlated, path separation reduces the effectiveness of the two color system in eliminating errors due to random fluctuations in atmospheric density along the propagation path. This may represent a fundamental limitation in the accuracy that can be obtained with two color systems. The problem boils down to determining how well the integrated atmospheric density along the two color paths is correlated.

Let L_1 and L_2 be the measured ranges at wavelengths λ_1 and λ_2. The actual range L is given by [13]

$$L \cong L_1 - \frac{n(\lambda_1)-1}{\Delta n_{21}} \Delta L_{21}$$

or (59)

$$L \cong L_2 + \frac{n(\lambda_2)-1}{\Delta n_{12}} \Delta L_{12}$$

where Δn_{12} and ΔL_{12} are the differences between the refractive index and measured path length.

Since the two laser beams will traverse slightly different paths in the atmosphere, the fluctuations on the two paths will be slightly decorrelated. Consequently, ΔL_{12} and ΔL_{21} will have a mean square error of

$$\langle[\Delta L(\lambda_1)-\Delta L(\lambda_2)]^2\rangle = 2(1-\rho_{12})\ \langle\Delta L^2\rangle \ . \tag{60}$$

ρ_{12} is the correlation coefficient of the path fluctuations and $\langle\Delta L^2\rangle$ is the mean square deviation on a single path.

The correlation coefficient can be calculated from the angular correlation function. Young [16] gives an expression for angular path separation as a function of the elevation angle ψ and the differential refractivity at the ranging site

$$\phi = \Delta n_{12} \cot \psi \ . \tag{61}$$

Equation (60) is actually the angular structure function defined in (16). Since the differential path lengths are multiplied by the coefficient in (59), the rms error in L caused by partially correlated path fluctuations is given by

$$L_{error} = \frac{n-1}{\Delta n} \left[D_{\Delta L}(\phi=\Delta n \cot \psi)\right]^{\frac{1}{2}} \tag{62}$$

The angular path separation can be decreased by decreasing Δn, i.e. by choosing the two frequencies close together. This decreases the value of the structure function and reduces L_{error}. However, the coefficient $(n-1)/\Delta n$ will be increased and this tends to increase the error. The dominant behavior of L_{error} as a function of Δn can be determined by noting that $\Delta n \cot \psi$ will be small compared to the correlation angle ϕ_s. The structure function can be approximated by the first term in its power series expansion to give (Sec. 2.3)

$$L_{error} \simeq (\Delta n)^{-1/6} (n-1) \beta^{1/2} \left(\frac{\cot \psi}{\phi_s}\right)^{5/6} \tag{63}$$

where β is a constant depending on the refractivity spectrum and C_n^2 profile. The overall error decreases as Δn increases. It is therefore desirable to make Δn large by choosing a large frequency difference.

The error reduction provided by a two color system can be estimated from equation (62) and the normalized structure functions plotted in Figures 12 and 14

$$\frac{L_{error}}{\Delta L_{rms}} = 2^{\frac{1}{2}} \frac{(n-1)}{\Delta n} \left[\frac{D_{\Delta L}(\phi=\Delta n \cot \psi)}{D_{\Delta L}(\pi)}\right]^{\frac{1}{2}} . \tag{64}$$

ΔL_{rms} is the rms deviation for a single frequency path. The ratio in equation (64) is plotted in Figure 16 as a function of the elevation angle ψ. The two color system is assumed to use the fundamental and frequency doubled output of a laser operating in the near infrared or visible wavelengths (λ_1 = 1 to .4μ, $\lambda_2 = \lambda_1/2$). Equation (42) (Figure 12) was used for the normalized structure function. At the low elevation angles near 10° the two color system shows little improvement over the single color system. For elevation angles over 30°, the two color system should provide at least an order of magnitude reduction in the path deviations.

Similar results would be obtained if the structure functions plotted in Figure 14 were used in (64). Figure 14 is based on Brookner's improved C_n^2 model (eq. (47)). If the Greenwood and Tarazano spectrum is used to calculate $D_{\Delta L}$ (curve b in Figure 12), the ratio in (64) is approximately 1/3 times the values given in Figure 16. Thus, the results in Figure 16 probably represent a lower bound for the expected improvement of two color systems over single color systems.

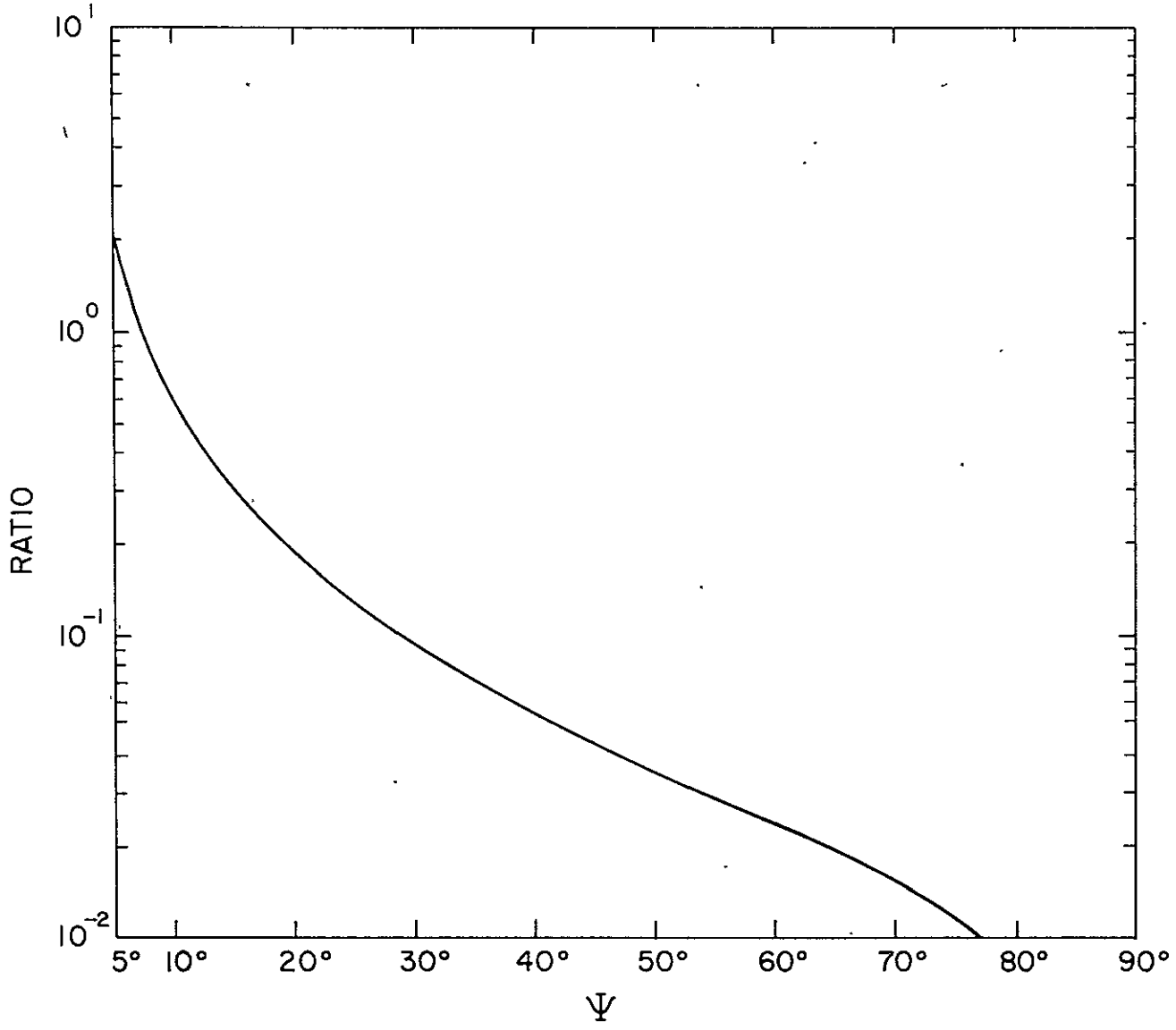

Figure 16. Ratio of the rms path deviation for a two-color system to the rms deviation for a single color system (eq. (64)). ψ is the satellite elevation angle. The results were calculated for $\lambda_1 = 2\lambda_2$ and apply to the case where $0.4\mu \leq \lambda_1 \leq 1\mu$.

For horizontal propagation Thayer [15] calculated the average separation between two line-of-sight rays with common endpoints,

$$\langle \Delta h \rangle \simeq \frac{L^2}{12} \left[\left(\frac{dn}{dh}\right)_{\lambda_1} - \left(\frac{dn}{dh}\right)_{\lambda_2} \right] \tag{65}$$

where L is the actual range. The error reduction provided by the two color system can be estimated using the parallel path structure function

$$\frac{L_{error}}{\Delta L_{rms}} \simeq 2^{\frac{1}{2}} \frac{(n-1)}{\Delta n} \left[\frac{D_{\Delta L}(d=\langle \Delta h \rangle)}{D_{\Delta L}(\infty)} \right] \tag{66}$$

Equation (66) is plotted in Figure (17) using the structure function given by (34). The outer scale of turbulence is on the order of 1 to 10 meters for propagation near the earth's surface. The two color system offers significant improvement over the shorter paths (<5 km). However, on the long paths where the path deviations can be large, the two color system shows little improvement over a single color system.

It should be noted that (66) gives only an approximate value for the ratio. The two color paths are not parallel; they are more closely approximated by circular arcs where $\langle \Delta h \rangle$ is the average arc separation. In (66) we have assumed the arc structure function can be approximated by the parallel path structure function evaluated at the average arc separation.

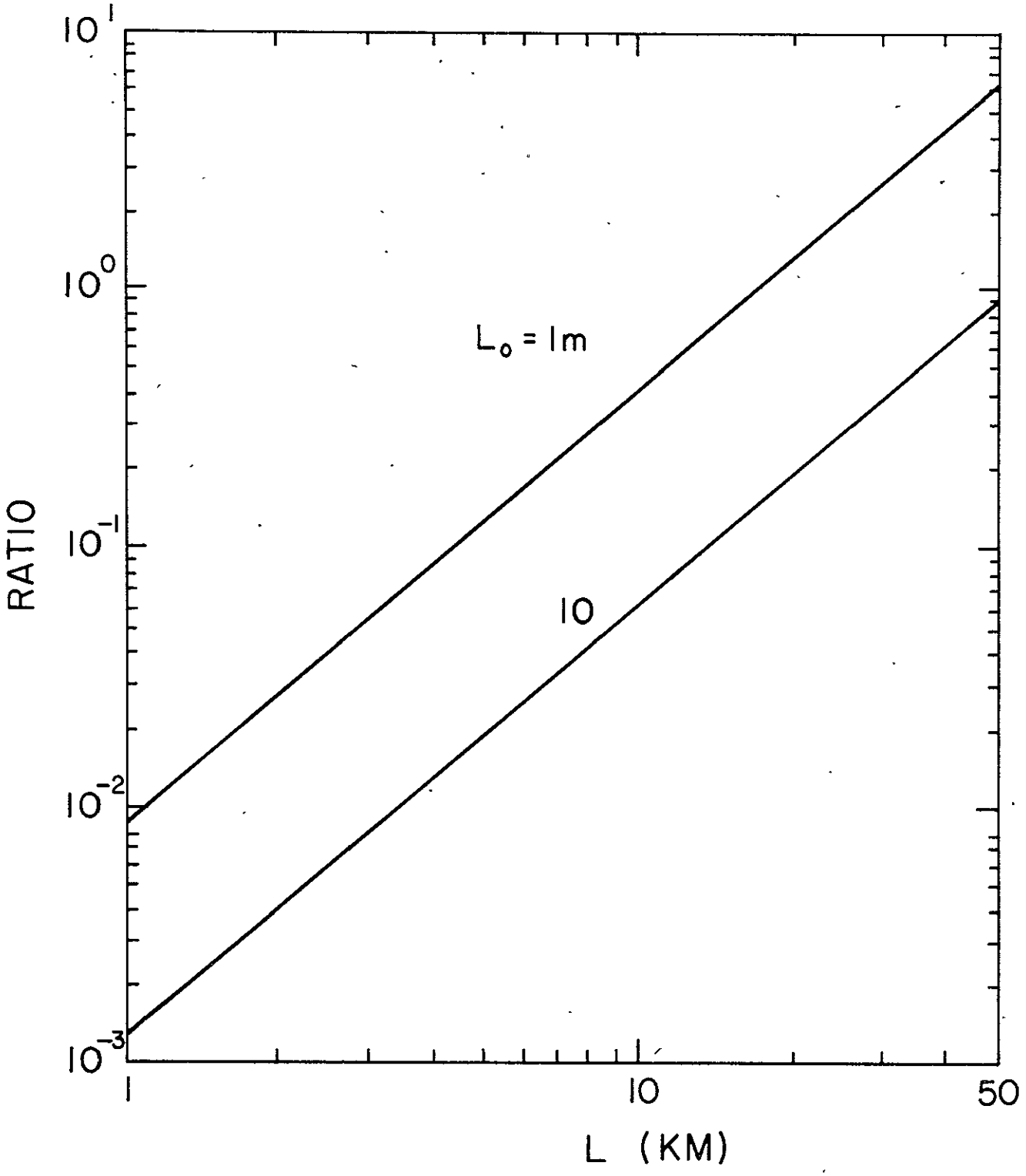

Figure 17. Ratio of the rms path deviation for a two-color system to the rms deviation for a single color system (eq. (66)). L is the actual range. The results were calculated for $\lambda_1 = 0.6328\mu$ and $\lambda_2 = 0.3164\mu$.

4. CONCLUSIONS

Atmospheric turbulence will introduce errors into distance measurements through a number of mechanisms. The most important is the random variations in the optical path length. The statistical properties of the path deviations were derived in Section 2. The rms path deviations will be typically a few millimeters or less. However, when the turbulence is strong ($C_n^2 \sim 10^{-13}$ $m^{-2/3}$) the deviations can be as high as a few centimeters.

It is possible to reduce the effects of the path deviations by averaging many different range measurements. Unfortuantely, the amount of reduction is limited by the long tails of the path deviation correlation functions. A substantial reduction in the deviations will be obtained only if the measurements are averaged over many correlation times (>10, see Sec. 3.1 and Fig. 15).

Two color systems can also be used to improve ranging accuracy. The difference between refraction at different wavelengths can be used to correct the range measurements for the effects of atmospheric refraction and turbulence. Over the shorter horizontal propagation paths ($\leq$10 km) and at the higher elevation angles (>30°), the two color systems can reduce the error caused by turbulence to a fraction of a millimeter or less. Over the long paths and at low elevation angles where the path deviations can be significant, the two color system will not perform much better than a single color system. In fact, the two color system can have a larger error in some cases (see Fig. 16 and 17).

The random path fluctuations caused by turbulence represent a fundamental limitation in the accuracy of both single color and two color ranging systems. When the turbulence is strong and the effective propagation path long, both systems can experience ranging errors approaching a few centimeters. When the turbulence is moderate or weak, the errors will be a millimeter or less.

APPENDIX A

Evaluation of $D_{\Delta L}(d)$ for the Greenwood and Tarazano Spectrum

The parallel path structure function can be calculated from equation (11)

$$D_{\Delta L}(d) = \alpha \int_0^\infty dK\ K\Phi_n^o(K)\ [1 - J_o(Kd)]. \qquad (A\text{-}1)$$

The integral in (A-1) is evaluated by rewritting the Bessel function in integral form and substituting the G-T spectrum (eq. (32)) for Φ_n^o

$$D_{\Delta L}(d) = \alpha' \frac{1}{\pi} \int_0^\pi d\theta \int_0^\infty dK\ K^{-5/6}(KL_o + 1)^{-11/6}\ (1 - e^{iKd\cos\theta}). \qquad (A\text{-}2)$$

The K integral can be expressed as a confluent hypergeometric function [19]

$$D_{\Delta L}(d) = \frac{\alpha'\Gamma(1/6)}{2^{1/6}}\ [U(1/6, -2/3, o) - \frac{1}{\pi} \int_o^\pi d\theta\, U(1/6, -2/3, -i\frac{d}{L_o}\cos\theta)] \qquad (A\text{-}3)$$

Since $J_o(Kd) \to o$ as $d \to \infty$ the normalized structure function is given by

$$\frac{D_{\Delta L}(d)}{D_{\Delta L}(\infty)} = 1 - \frac{\frac{1}{\pi}\int_o^\pi d\theta\ U(1/6, -2/3, -i\frac{d}{L_o}\cos\theta)}{U\ (1/6, -2/3, o)}\ . \qquad (A\text{-}4)$$

When d/L_o is small, U can be expanded in a power series [20]

$$\frac{D_{\Delta L}(d)}{D_{\Delta L}(\infty)} = \sum_{m=o}^{\infty} [a_m(\frac{d}{L_o})^{m+5/3} + b_m(\frac{d}{L_o})^{2(m+1)}] \qquad (A\text{-}5)$$

Where

$$a_o = \frac{\Gamma(11/6)\Gamma(-2/3)}{\Gamma(1/6)\Gamma(8/3)} \frac{1}{\pi} \int_o^{\pi} d\theta \, (-i \cos\theta)^{5/3} = 0.2093$$

$$a_1 = \frac{\Gamma(11/6)\Gamma(-2/3)}{\Gamma(1/6)\Gamma(8/3)} \frac{11}{16} \frac{1}{\pi} \int_o^{\pi} d\theta \, (-i \cos\theta)^{8/3} = 0.1844$$

$$a_2 = \frac{\Gamma(11/6)\Gamma(-2/3)}{\Gamma(1/6)\Gamma(8/3)} \frac{17}{64} \frac{1}{\pi} \int_o^{\pi} d\theta \, (-i \cos\theta)^{11/3} = -0.0404$$

$$b_o = \frac{\Gamma(11/6)\Gamma(-2/3)}{\Gamma(1/6)\Gamma(8/3)} \left(\frac{-7}{32}\right) = -0.2188$$

$$b_1 = \frac{\Gamma(11/6)\Gamma(-2/3)}{\Gamma(1/6)\Gamma(8/3)} \frac{13 \times 19}{8\pi} \left[\frac{\Gamma(5/2)}{4!}\right]^2 = 0.0302 \qquad \text{(A-6)}$$

APPENDIX B

Evaluation of the Angular Structure Function

When the angle ϕ is small, the cosine in (16) is approximately one and the tangent can be approximated by its argument. In this case the angular structure function $D_{\Delta L}(\phi)$ can be written in terms of the parallel path structure function $D_{\Delta L}(d)$

$$\frac{D_{\Delta L}(\phi)}{D_{\Delta L}(\pi)} = \frac{\int_0^L d\xi\ B_n^{\nu}(\xi) \int_0^{\infty} dK\ K\phi_n^{o}(K)\ [1-J_o(K\phi\xi)]}{\int_0^L d\xi\ B_n^{\nu}(\xi)}$$

$$= \frac{\int_0^L d\xi\ B_n^{\nu}(\xi)\cdot D_{\Delta L}(d=\xi\phi)}{\int_0^L d\xi\ B_n^{\nu}(\xi)\ D_{\Delta L}(\infty)} \quad . \tag{B-1}$$

The power series expansion of $D_{\Delta L}(d)/D_{\Delta L}(\infty)$ for the G-T spectrum was derived in Appendix B

$$\frac{D_{\Delta L}(d)}{D_{\Delta L}(\infty)} = \sum_{m=o}^{\infty} [a_m (\frac{d}{L_o})^{m + 5/3} + b_m (\frac{d}{L_o})^{2(m+1)}]. \tag{B-2}$$

The values of the first few coefficients $\{a_m\}$ and $\{b_m\}$ are calculated in Appendix B. After substituting (B-2) into (B-1) we obtain

$$\frac{D_{\Delta L}(\phi)}{D_{\Delta L}(\pi)} = \sum_{m=o}^{\infty} [a_m (\frac{\phi}{L_o})^{m + 5/3} \int_0^L d\xi\ \xi^{m + 5/3}\ B_n^{\nu}(\xi)$$

$$+ b_m (\frac{\phi}{L_o})^{2(m+1)} \int_0^L d\xi\ \xi^{2(m+1)}\ B_n^{\nu}(\xi)]. \tag{B-3}$$

If C_n^2 is described by the exponential model given in (21), (B-3) becomes

$$\frac{D_{\Delta L}(\phi)}{D_{\Delta L}(\pi)} = \sum_{m=o}^{\infty} [a_m \Gamma(m + 8/3) (\phi/\phi_s)^{m + 5/3} + b_m \Gamma(2m + 3) (\phi/\phi_s)^{2(m + 1)}] \tag{B-4}$$

where $\phi_s = \frac{L_o \sin \psi}{h_s}$. The small ϕ asymptote is given by the first term in the series

$$\frac{D_{\Delta L}(\phi << \phi_s)}{D_{\Delta L}(\infty)} \simeq a_o \Gamma(8/3) (\phi/\phi_s)^{5/3} = 0.315 (\phi/\phi_s)^{5/3}. \tag{B-5}$$

APPENDIX C

Evaluation of the Angular Correlation Function

To evaluate the angular correlation function using Brookner's model for C_n^2 (eq. (47)), we start with equation (B-1) in Appendix B and relation (33) to obtain

$$R_{\Delta L}(\phi) = \frac{\int_0^L d\xi\ B_n^{\nu}(\xi)\ R_{\Delta L}(d=\xi\phi)}{\int_0^L d\xi\ B_n^{\nu}(\xi)} . \qquad \text{(C-1)}$$

The parallel path correlation function calculated using the von Karman spectrum is given by (25) with $\mu = 11/6$

$$R_{\Delta L}(d) = \frac{2^{1/6}}{\Gamma(5/6)} \left(\frac{d}{L_o}\right)^{5/6} K_{5/6}\left(\frac{d}{L_o}\right) . \qquad \text{(C-2)}$$

For Brookner's model, the integrated contributions of C_n^2 due to the lower atmosphere and the tropopause are defined as

$$C_n^+ + C_{nT}^+ = \int_o^{\infty} dh\ C_n^2(h)$$

(C-3)

$$C_n^+ = \int_o^{\infty} dh\ C_{no}^2\ h^{-b}\ e^{-h/hs} = C_{no}^2\ h_s^{(1-b)}\ \Gamma(1-b)$$

Using equations (C-2), (C-3) and (47) in (C-1) gives

$$R_{\Delta L}(\phi) = \frac{C_n^+}{(C_n^+ + C_{nT}^+)} \frac{2^{1/6}\csc\psi}{\Gamma(1-b)\ \Gamma(5/6)} \int_o^{\infty} du\ u^{-b}\ e^{-u} \left(\frac{\phi}{\phi_s} u\right)^{5/6} K_{5/6}\left(\frac{\phi}{\phi_s} u\right)$$

$$+ \frac{C_{nT}^+}{(C_n^+ + C_{nT}^+)} \frac{2^{1/6}}{\Gamma(5/6)} \left(\frac{\phi}{\phi_T}\right)^{5/6} K_{5/6}\left(\frac{\phi}{\phi_T}\right) \qquad \text{(C-4)}$$

where ϕ_s and ϕ_T are the lower atmosphere and tropopause correlation angles defined in (49). The integral in (C-4) can be written in terms of a hypergeometric function using the integral relation given in Gradshteyn and Ryzik [17] and the transformations given in Abramowitz and Stegun [18]. The resulting expression for the angular correlation function is

$$R_{\Delta L}(\phi) = \frac{C_n^+}{(C_n^+ + C_{nT}^+)} \beta_o \; {}_2F_1(\tfrac{1}{2}-b/2,\ 1-b/2,\ 7/3-b,\ 1-\phi^2/\phi_s^2)$$

$$+ \frac{C_{nT}^+}{(C_n^+ + C_{nT}^+)} \beta_1 (\phi/\phi_T)^{5/6} K_{5/6}(\phi/\phi_T),\ b<1 \qquad \text{(C-5)}$$

where

$$\beta_o = \frac{\sqrt{\pi}}{\Gamma(5/6)} \frac{\Gamma(8/3-b)}{\Gamma(7/3-b)} \frac{1}{2^{5/3-b}} \qquad \text{(C-6)}$$

$$\beta_1 = \frac{2^{1/6}}{\Gamma(5/6)}$$

REFERENCES

1. V.I. Tatarski, The Effects of the Turbulent Atmosphere on Wave Propagation, (National Technical Information Service, 1971).

2. A Ishimaru, "A new approach to the problem of wave fluctuations in localized smoothly varying turbulence," IEEE Trans. Ant. Prop., AP-21, 47 (1973).

3. J. Bufton, "A Radiosonde Thermal Sensor Technique for Measurement of Atmospheric Turbulence," NASA Tech. Rep. G-7443 (November 1973).

4. J. Bufton, "Comparison of vertical profile turbulence structure with stellar observations," Applied Optics, 12, 1785 (1973).

5. E. Brookner, "Improved model for the structure constant variations with altitude," Applied Optics 10, 1960 (1971).

6. P. Titterton, "Scintillation and transmitter-aperture averaging over vertical paths," J. Opt. Soc. Amer., 63, 439 (1973).

7. I. S. Gradshteyn and I. W. Ryzhik, Table of Integrals Series and Products, (Academic Press, 1965), eq. 3.197-5.

8. D. P. Greenwood and D. O. Tarazano, "A proposed form for the atmospheric microtemperature spatial spectrum in the input range," RADC Tech. Rep. RADG-TR-74-19, (February 1974).

9. R. E. Hufnagel, Restoration of Atmospherically Degraded Images, Woods Hole Summer Study, (1966), Vol. 2, Appendix 3, p. 15.

10. J. W. Marini and C. W. Murray, "Correction of laser range tracking data for atmospheric refraction at elevations above 10 degrees," NASA Tech. Rep. X-591-73-351 (November 1973).

11. J. Saastamoinen, "Contributions to the theory of atmospheric refraction," Bulletin Geodesiqne, 105-107, pp. 279-298, 383-397, 13-34 (1972).

12. J. Marini, "Correction of satellite tracking data for an arbitrary tropospheric profile," Radio Science, 7, 223 (1972).

13. P. L. Bender and J. L. Owens, "Correction of optical distance measurements for the fluctuation atmospheric index of refraction," J. Geophysical Res., 70, 2461 (May 1965).

14. K. B. Earnshaw and E. N. Hernandez, "Two-laser optical distance measuring instrument that corrects for the atmospheric index of refraction," Applied Optics, 11, 749 (1972).

15. G. D. Thayer, "Atmospheric effects on multiple-frequency range measurements," ESSA Tech. Rep. IER 56-ITSA53 (October 1967).

16. A. T. Young, "Photometeric error analysis. VIII. the temporal power spectrum of scintillation," Applied Optics, 8, 869 (1969).

17. Reference [7], eq. 6.621-3.

18. M. Abramowitz and I. A. Stegun, Handbook of Mathmetical Functions, (Dover Publications, 1970), eqs. 15.3.26 and 15.3.3.

19. Reference [18], eq. 13.2.5.

20. Reference [18], eqs. 13.1.2 and 13.1.3.